WATER RESOURCES RESEARCH, VOL. 49, 7778–7796, doi:10.1002/2013WR014012, 2013

Groundwater age distributions at a public drinking water supply well field derived from multiple age tracers (^{85}Kr, ^{3}H/^{3}He, and ^{39}Ar)

Ate Visser,[1] Hans Peter Broers,[2,3,4] Roland Purtschert,[5] Jürgen Sültenfuß,[6] and Martin de Jonge[4,7]

Received 23 April 2013; revised 19 September 2013; accepted 10 November 2013; published 27 November 2013.

[1] Groundwater age is a key aspect of production well vulnerability. Public drinking water supply wells typically have long screens and are expected to produce a mixture of groundwater ages. The groundwater age distributions of seven production wells of the Holten well field (Netherlands) were estimated from tritium-helium (^{3}H/^{3}He), krypton-85 (^{85}Kr), and argon-39 (^{39}Ar), using a new application of a discrete age distribution model and existing mathematical models, by minimizing the uncertainty-weighted squared differences of modeled and measured tracer concentrations. The observed tracer concentrations fitted well to a 4-bin discrete age distribution model or a dispersion model with a fraction of old groundwater. Our results show that more than 75% of the water pumped by four shallow production wells has a groundwater age of less than 20 years and these wells are very vulnerable to recent surface contamination. More than 50% of the water pumped by three deep production wells is older than 60 years. ^{3}H/^{3}He samples from short screened monitoring wells surrounding the well field constrained the age stratification in the aquifer. The discrepancy between the age stratification with depth and the groundwater age distribution of the production wells showed that the well field preferentially pumps from the shallow part of the aquifer. The discrete groundwater age distribution model appears to be a suitable approach in settings where the shape of the age distribution cannot be assumed to follow a simple mathematical model, such as a production well field where wells compete for capture area.

Citation: Visser, A., H. P. Broers, R. Purtschert, J. Sültenfuß, and M. de Jonge (2013), Groundwater age distributions at a public drinking water supply well field derived from multiple age tracers (^{85}Kr, ^{3}H/^{3}He, and ^{39}Ar), *Water Resour. Res.*, *49*, 7778–7796, doi:10.1002/2013WR014012.

1. Introduction

[2] It is estimated that one third of the world's population is dependent on groundwater [*WHO*, 2006]. In the Netherlands, groundwater provides drinking water to 68% of the population. Groundwater systems are under pressure of overdraft and contamination, most commonly nitrate [*Foster et al*., 1982; *Nolan et al*., 1997; *Spalding and Exner*, 1993; *Strebel et al*., 1989]. If nitrate concentrations in the pumped groundwater exceed the drinking water limit, it needs to be treated. If treatment is not economically feasible, wells are often abandoned.

[3] While European legislation is aimed at reducing the nitrate pressure on groundwater and improving groundwater quality [*EU*, 2006], many wells are threatened by rising nitrate concentrations due to the long travel times of contaminants through the subsurface [*Batlle-Aguilar et al*., 2007]. Subsurface travel times—in this paper, referred to as groundwater age [*Etcheverry and Perrochet*, 2000]—are a key aspect of well vulnerability [*Manning et al*., 2005]. The trends in groundwater quality depend on the historical load of nitrate at the land surface [*Böhlke*, 2002; *Broers and Van der Grift*, 2004; *Visser et al*., 2009b], the reactivity of the sediments to attenuate nitrate [*Green et al*., 2010; *Landon et al*., 2011; *Zhang et al*., 2009] and the groundwater age [*Broers and Van Geer*, 2005; *Broers et al*., 2007; *Duffy and Lee*, 1992; *Laier*, 2004; *Osenbrück et al*., 2006; *Van der Velde et al*., 2012; *Visser et al*., 2009a]. These three factors combined complicate the direct interpretation of trends in pumped groundwater production wells [*Broers and Van Geer*, 2005]. Independent assessment of contaminant loads, geochemistry, and groundwater ages is therefore the key to understanding contaminant trends in groundwater production wells. This study focused on determining the groundwater age distribution of a pumped drinking water production well field from multiple age tracers.

[1]Lawrence Livermore National Laboratory, Livermore, California, USA.
[2]Deltares, Unit Soil and Groundwater Systems, Utrecht, Netherlands.
[3]TNO, Geological Survey of the Netherlands, Utrecht, Netherlands.
[4]Critical Zone Hydrology Group, VU University, Amsterdam, Netherlands.
[5]Climate and Environmental Physics, University of Bern, Bern, Switzerland.
[6]Department of Oceanography, Institute of Environmental Physics, Universität Bremen, Bremen, Germany.
[7]Vitens Water, Zwolle, Netherlands.

Corresponding author: A. Visser, Lawrence Livermore National Laboratory, 7000 East Ave., Livermore, CA 94550, USA. (visser3@llnl.gov)

0043-1397/13/10.1002/2013WR014012

[4] Groundwater production wells typically have long screens and are expected to produce a mixture of groundwater travel times [*Manning et al*., 2005]. The groundwater travel time distribution can be derived from tracer concentrations, and conceptual or numerical models. Analytical or numerical groundwater flow and transport models delineate well capture zones [*Cole and Silliman*, 1997, 2000; *Frind et al*., 2002; *Rock and Kupfersberger*, 2002], assess well vulnerability [*Eberts et al*., 2012; *Harrar et al*., 2003; *Mendizabal and Stuyfzand*, 2011] and derive the age distribution of groundwater pumped by the wells [*Molénat and Gascuel-Odoux*, 2002; *Visser et al*., 2009c]. Ideally, these models are calibrated against environmental tracers for groundwater age [*Sanford*, 2011; *Troldborg et al*., 2008; *Zuber et al*., 2011].

[5] The age distribution of a well cannot be determined independently from a single age tracer. Therefore, a multitracer approach is required to capture the groundwater age distribution of a well from tracer data alone [*Corcho Alvarado et al*., 2007; *Plummer et al*., 2001; *Sültenfuß et al*., 2011]. At the time scale relevant for well vulnerability and response to anthropogenic contamination (years to decades), a number of age tracers are suitable: krypton-85 (^{85}Kr) [*Smethie et al*., 1992], tritium-helium (^{3}H/^{3}He) [*Poreda et al*., 1988; *Schlosser et al*., 1988], chlorofluorocarbons (CFCs) [*Busenberg and Plummer*, 1992], sulfurhexafluoride (SF_6) [*Busenberg and Plummer*, 2000], and argon-39 (^{39}Ar) [*Loosli*, 1983; *Loosli et al*., 1989; *Oeschger et al*., 1974]. Mathematical models representing typical groundwater flow systems [*Maloszewski and Zuber*, 1993, 1998] are available to convert the tracer concentrations to the age distribution [*Corcho Alvarado et al*., 2007; *Ivey et al*., 2008; *Massoudieh et al*., 2012; *Purtschert et al*., 1999] using software like Lumpy [*Suckow*, 2012] or TracerLPM [*Jurgens et al*., 2012]. These software programs enable the user to find groundwater age distributions that reproduce measured tracer concentrations, by minimizing the residuals between measured and modeled concentrations. At a public drinking water supply well field, consisting of multiple production wells pumping at different depths and locations in close proximity, wells compete for the capture area of the entire well field and mathematical models representing isolated wells may not be a valid assumption for the age distribution of the pumped groundwater of individual wells within the well field. A shape-free model [*Cirpka et al*., 2007]—or age histogram—can describe age distributions that capture a broader range of possibilities than a particular analytical solution. The shape-free age distribution has been successfully derived for a production well near a river from times series of electric conductivity of groundwater and river water [*Cirpka et al*., 2007]. This study investigated whether a limited number of tracers collected at a single moment are sufficient to derive a unique solution of a discrete nonanalytical age distribution.

[6] In this study, groundwater age distributions from the drinking water production well field near Holten (Netherlands) were investigated, based on tritium, helium isotopes, ^{85}Kr and ^{39}Ar activities, using a discrete age distribution (age histogram) approach. In addition, existing analytical models were fitted to measured tracer concentrations and compared to the shape of the age histogram.

[7] ^{3}H/^{3}He samples from monitoring wells surrounding the well field were analyzed to (1) evaluate whether the reconstructed historical concentrations of tritium in precipitation are representative for the study site and (2) establish the vertical age profile in the aquifer (age stratification). The age stratification was compared with the age distributions derived from the production wells to evaluate whether the well field evenly captures groundwater from the entire depth of the aquifer or preferentially samples certain depths ranges of the aquifer.

[8] In a homogeneous unconfined aquifer with a fully penetrating monitoring well or a pumped production well with sufficient flow to capture the entire thickness of the aquifer, the age stratification follows a logarithmic profile and the pumped groundwater corresponds to an exponential groundwater age distribution model [*Broers and Van Geer*, 2005; *Vogel*, 1967]. We hypothesize that the Holten well field as a whole acts as a pumped production well with sufficient flow to capture the entire thickness of the aquifer. We therefore state that the age stratification in the aquifer follows a logarithmic profile (Hypothesis A), and that the age distribution for the entire well field as a whole is exponential and consistent with the logarithmic age profile in the aquifer (Hypothesis B). We also state that the production wells influence each other by competing for capture area and, as a result, the groundwater age distributions produced by individual production wells differ from each other and from the well field as a whole (Hypothesis C).

[9] The following sections describe the Holten well field and its hydrogeological setting, the sampling and analytical procedures, the methods to derive the groundwater age distribution, the analytical results of the collected samples and the derived age distributions, a discussion of the validity of our hypotheses, the expected benefits of additional tracers and numerical approaches, and the drinking water well vulnerability and predicted responses to well field management changes.

2. Methods

2.1. Hydrogeological Setting of the Holten Production Well Field

[10] The production well field is located near Holten, in the eastern part of the Netherlands. The area is characterized by the Holterberg, an ice-pushed ridge north of Holten, consisting of thrusted sediments reaching 70 m above mean sea level (msl). The surface elevation in the rest of the area varies between 15 and 20 m above msl. A phreatic groundwater system is present in the (partly ice pushed) fluvial and periglacial deposits of 90–120 m thickness [*Griffioen et al*., 2003; *Ruijpers et al*., 2004]. The hydrological base of the aquifer is formed by the Breda Formation (Tertiary marine sediments) at a depth of approximately 70–100 m below sea level. The ice-pushed ridge, north of the well field, is forested. Land use is mostly agricultural to the south, west, and east of the well field [*Griffioen et al*., 2003; *Ruijpers et al*., 2004].

[11] The Holten well field produces groundwater at a rate of 2.5 million cubic meters per year from a depth of 10–70 m below the surface. The well field is vulnerable to contamination because of the agricultural land use and residential areas in the capture area, the sandy aquifer,

expected short groundwater residence times and groundwater levels at 4–8 m below surface. Nitrate and agriculture related contaminants like heavy metals are the largest threat to the water quality in the production wells.

[12] The Holten well field has been the subject of a number of prior investigations, involving the well field capture area [*Iwaco*, 1993], groundwater quality in relation to the contaminant load and geochemical processes [*Griffioen et al*., 2002], and a coupled transport model was used to assess the status and development of contaminants in the pumped groundwater [*Griffioen et al*., 2003]. The transport model was later extended to a 3-D coupled reactive transport model [*Ruijpers et al*., 2004]. A groundwater quality negotiation support system was studied to change land use management in the vicinity of the well field [*Van den Brink et al*., 2008].

[13] The well field currently has 19 pumped production wells with a capacity of approximately 33 m^3/h each (Table 1). The total production capacity of 625 m^3/h is required to meet peak demand, but not all wells are operated continuously. The first production well was constructed in 1901. The oldest currently active production well was constructed in 1959. Most production wells were constructed between 1960 and 1973 and are screened between 15 and 30 m below the surface, referred to as "shallow wells." In 1985, three deep production wells were drilled and screened from 45 to 70 m below the surface. These wells were intended to capture deep iron-rich anoxic groundwater to prevent well clogging that occurs when shallow oxic groundwater mixes with deep anoxic groundwater.

[14] The three deep production wells of the well field (Figure 1) are screened in the fine sandy sediments of the Oosterhout Formation (−10 to −70 m msl). The Oosterhout Formation has a high hydraulic conductivity and contains sparse clayey and loamy lenses with thicknesses of several meters. At the Holten well field, the Oosterhout Formation is intersected by coarse channel-fill sediments of the Appelscha Formation. The shallow production wells of the well field are predominantly screened in the Urk Formation (coarse sands deposited by the river Rhine, +10 to −5 m msl). South of the Holterberg, a thin unit (∼1 m) of coarse and gravely deposits (Peize Formation) from former Baltic rivers exists below the Urk Formation. These formations have a very high hydraulic conductivity. Fluvioglacial fine to coarse sands of the Drenthe Formation, approximately 10 m thick, are at the surface at the Holten well field.

[15] Periglacial channel-fill deposits (Boxtel Formation), varying from silty clay to coarse, gravely sands are found at the surface south of the Holten well field (not shown in Figure 1). The Boxtel Formation has a moderately high hydraulic conductivity and within the upper few meters local loamy or clayey lenses, originating from moraine deposits, occur.

2.2. Well Selection, Sampling, and Measurements

[16] Eleven production wells were selected for sampling based on their typical production, ensuring that both shallow and deep production wells in close proximity were sampled. Samples for $^3H/^3He$ analysis were collected from all 11 wells, providing over 95% of the total production. Samples for ^{85}Kr, ^{39}Ar, dissolved gas and water stable iso-

Table 1. Characteristics of the Production Wells, Analytical Results, and Apparent Ages

ID	Top (m below surface)	Bottom (m below surface)	Production (m^3/d)	Date (dd-mm-yy)	ΔNe (%)	^{85}Kr (dpm/ccKr)	± (dpm/ccKr)	^3H (TU)	± (TU)	$^3He_{trit}$ (TU eq.)	± (TU eq.)	^{39}Ar (% modern)	± (% modern)	$^4He_{rad}$ (10^{-6}ccSTP/L)	± (10^{-6}ccSTP/L)	δ^2H (‰ VSMOW)	$\delta^{18}O$ (‰ VSMOW)	^{85}Kr age (year)	± (year)	$^3H/^3He$ age (year)	± (year)	^{39}Ar age (year)	± (year)
59-05	19	30	800	20-04-10	−7	38	1.2	6.48	0.14	21.1		100	10	0.0		−48.54	−7.35	12	0.3	25.7	–	0	39
61-08	13	32	67	20-04-10	−23			7.4	0.15	27.4				0.0						27.5	–		
67-19	14	23	530	21-04-10	26	39.7	1.5	6.09	0.15	6.4	0.5	104	8	0.1	0.33	−48.98	−7.41	12	0.3	12.7	0.8	0	30
71-20	21	30	530	20-04-10	19			6.16	0.15	19.5	0.5			0.0	0.35					25.4	0.5		
72-22	15	34	530	20-04-10	20	35.9	1.3	6.75	0.16	14.0	0.5	93	6	0.0	0.34	−47.71	−7.24	13	0.4	20.0	0.5	28	25
72-27	13	28	530	20-04-10	−22			6.44	0.23	25.3				0.0						28.3	–		
73-29	16	31	800	20-04-10	13	39.4	1.6	6.38	0.16	8.7	0.5	100	10	0.0	0.34	−48.25	−7.26	12	0.4	15.3	0.7	0	39
85-33	46	68	800	20-04-10	17	2.7	0.2	1.23	0.05	9.2	0.5	51	8	11.0	0.35	−48.62	−7.18	39	0.8	38.0	1.1	261	61
85-34	48	74	800	21-04-10	6	8.4	0.5	3.98	0.11	21.1	0.5	77	7	6.6	0.36	−49.20	−7.35	27	0.4	32.7	0.6	101	35
85-35	45	75	800	21-04-10	16	8.7	0.3	3.82	0.11	20.4	0.5	74	6	4.5	0.36	−49.11	−7.34	27	0.3	32.8	0.6	117	31
04-38	37	46	800	20-04-10	5			5.98	0.15	23.6	0.5			0.0	0.35					28.4	0.5		

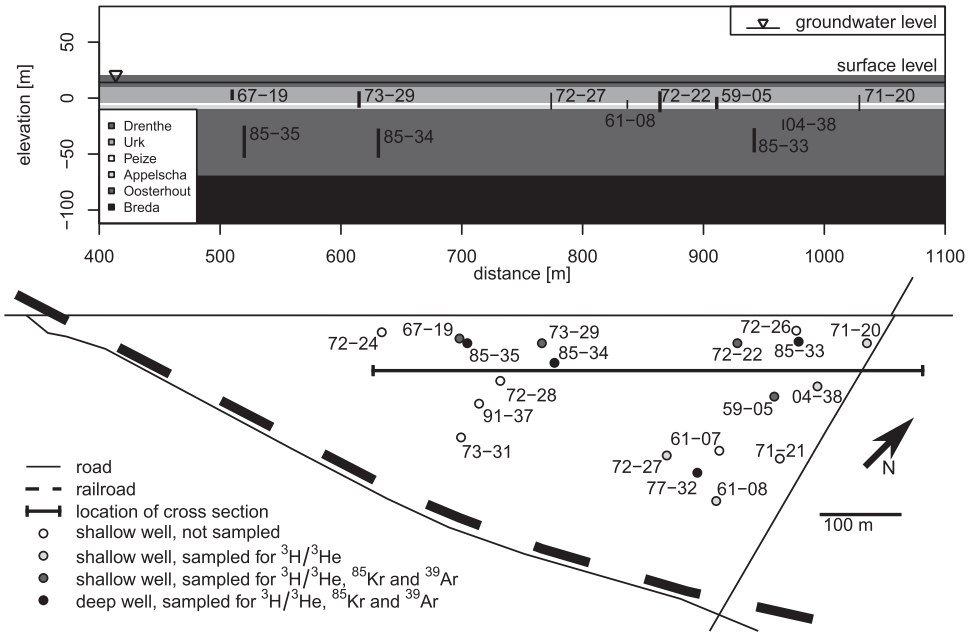

Figure 1. Cross section and map of the Holten public drinking water production well field.

tope analysis were collected from 7 of the 11 wells, capturing 69% of the total drinking water production.

[17] Samples were collected on 20 and 21 April 2010 from a sample port at the well head during regular well production. Tritium samples were collected in duplicate in 500 mL plastic bottles. Samples for helium and neon isotopes were collected in duplicate in copper tubes, following the sampling protocol of the Bremen University (http://www.noblegas.uni-bremen.de/documents/sampling_hints.pdf). $^3H/^3He$ samples were collected from three monitoring screens in the casing of production well 85-35 by an inertia foot valve pump. The outlet of the sample line was elevated 3 m to provide some back pressure during the downward motion of the inertia pump. $^3H/^3He$ samples were measured at the Bremen Mass Spectrometric Facility for the measurement of Helium Isotopes, Neon, and Tritium in Water [*Sültenfuß et al*., 2004]. ^{39}Ar and ^{85}Kr samples were collected by degassing 2–4 m^3 of water at the well head. ^{39}Ar and ^{85}Kr activities were measured by low level gas proportional counting in the Deep Laboratory of the Physics Institute, University of Bern, Switzerland [*Loosli*, 1983]. The major gas composition (nitrogen, oxygen, argon, carbon dioxide, methane) of the extracted gas was measured prior to the separation of krypton and argon by gas chromatography. Stable isotope samples were collected in 200 mL glass bottles and analyzed at the University of Bern.

[18] To study the age distribution of the groundwater produced by the entire well field, tracer concentrations of the pumped mixture from all the production wells were calculated from the separate production well samples. The production well samples were weighted to ensure that the relative contribution of shallow (63%) and deep (37%) wells to the total production was well represented by the average tracer concentrations. For example, the weight of shallow well i ($W_{S,i}$) is calculated from the production (P) of well i, the sum of the production of all shallow wells ($\Sigma P_{S,sampled}$), the sum of the production of all shallow wells (ΣP_S) and the well field as a whole (ΣP_W) (equation (1)):

$$W_{S,i} = \frac{P_i}{\sum P_{S,\text{sampled}}} \frac{\sum P_S}{\sum P_W} \tag{1}$$

[19] The drinking water production well field is surrounded by a network of multilevel monitoring wells with short screens (1–2 m) (Table 2) to measure water level fluctuations and monitor water quality parameters. Eight multilevel wells (26 screens total) of the monitoring network were sampled in May 2010 for tritium, helium isotopes, and noble gases to provide the age stratification in the aquifer. Tritium samples were collected in 500 mL plastic bottles using an inertia foot valve pump. Helium isotope and noble gas samples were collected by advanced diffusion samplers [*Gardner and Solomon*, 2009] from 22 screens. The total dissolved gas pressure (TDG) was measured at the screen depth of the monitoring well using a TDG probe [*Manning et al*., 2003; *Visser et al*., 2007] and again in the advanced diffusion samplers in the laboratory. Nine noble gas samples were repeated in March 2011 because the previous results showed incomplete equilibration with well water. Tritium samples were repeated at the same time. Noble gases and nitrogen were analyzed at the University of Utah dissolved and noble gas laboratory. Tritium samples were measured in Bremen [*Sültenfuß et al*., 2004].

2.3. Data Interpretation

2.3.1. Noble Gas Dissolution Models

[20] The noble gases measured in the advanced diffusion samplers were fitted to five excess air and degassing models (unfractionated air (UA) [*Heaton and Vogel*, 1981], closed equilibrium (CE) [*Aeschbach-Hertig et al*., 1999], partial reequilibration (PR) [*Aeschbach-Hertig et al*., 2000; *Stute et al*., 1995], equilibrium degassing (ED) [*Aeschbach-Hertig et al*., 2008; *Visser et al*., 2007], and diffusive

Table 2. Characteristics of the Monitoring Wells, Analytical Results, and Apparent $^3H/^3He$ Ages

ID	Screen	Top (m below surface)	Bottom (m below surface)	gwl (m below surface)	Date (dd-mm-yy)	^3H (TU)	± (TU)	ΔNe (%)	$^4He_{rad}$ (10^{-6} ccSTP/L)	± (10^{-6} ccSTP/L)	$^3He_{trit}$ (TU eq)	± (TU eq)	age[a] (year)	± (year)
28CA3309	2	−11	−12	−7.0	31-05-10	7.56	0.18							
28CA3309	3	−13	−14	−7.0	31-05-10	6.44	0.15	20	0	0.35	3.5	0.5	7.8	1.0
28CA3309	4	−16	−17	−7.0	31-05-10	6.14	0.15	21	0	0.35	3.7	0.5	8.3	1.0
28CA3336	2	−10	−11	−4.3	27-05-10	6.54	0.15							
28CA3336	3	−13	−14	−4.3	27-05-10	6.12	0.15	−24	0	-	8.8	0.4	15.9	0.6
28CA3336	4	−15	−16	−4.3	27-05-10	6.24	0.14	−12	0	-	18.2	0.4	24.3	0.5
28CP0168	2	−20	−25	−7.9	26-05-10	9.58	0.21	3	0	0.35	51.4	0.5	32.9	0.4
28CP0196	1	−9	−11	−2.1	01–06-10	6.27	0.15	11	0	0.34	4.3	0.5	9.3	1.0
28CP0196	3	−23	−25	−2.0	01–06-10	13.04	0.27	13	0	0.35	102.7	0.5	38.8	0.3
28CP0207	1	−8	−10	−1.5	01–06-10	6.07	0.14	−43	0	-	21.7	0.4	27.0	0.8
28CP0207	3	−23	−25	−1.5	01–06-10	3.91	0.10	−1	0	-	28.5	0.5	37.6	0.5
28CP0245	1	−11	−12	−5.6	26-05-10	6.35	0.14	25	0	0.34	3.4	0.5	7.6	1.2
28CP0245	2	−20	−22	−5.6	26-05-10	7.12	0.17	18	0	0.34	25.4	0.5	27.0	0.4
28CP0245	3	−56	−58	−5.6	26-05-10	0.01	0.02	10	0.68	0.33	3.0	0.5	101.6	8.8
28CP0248	1	−6	−7	−3.6	31-05-10	7.19	0.16	−4	0	-	0.3	0.4	0.8	0.9
28CP0248	2	−11	−12	−4.1	31-05-10	5.97	0.12	−37	0	-	8.3	0.4	15.5	0.7
28CP0248	3	−22	−23	−3.7	23-03-11	8.47	0.17	−52	0	-	35.6	0.4	29.3	0.5
28CP0250	1	−21	−22	−8.3	26-05-10	9.92	0.21	−15	0	-	41.2	0.4	29.1	0.4
28CP0250	2	−30	−31	−7.9	23-03-11	7.05	0.14	−6	0	-	34.0	0.4	31.3	0.4
28CP0250	3	−44	−45	−7.8	23-03-11	0.76	0.03	10	0	0.34	32.9	0.5	67.4	0.7
28CP0267	1	−13	−15	−8.5	23-03-11	6.31	0.13	17	0	0.35	2.2	0.5	5.3	1.1
28CP0267	2	−24	−26	−8.5	23-03-11	6.21	0.13	32	0	0.34	21.5	0.5	26.6	0.4
28CP0267	3	−30	−32	−8.5	23-03-11	7.17	0.13	18	2.3	0.34	35.5	0.5	31.7	0.3
28CP0267	4	−38	−40	−8.4	23-03-11	9.23	0.17	50	0	0.34	73.4	0.5	39.0	0.3
28CP0267	5	−51	−53	−8.7	28-05-10	0.03	0.02							
28CP0268	1	−9	−11	−4.9	31-05-10	6.93	0.15	24	0	0.34	14.3	0.5	19.9	0.5
28CP0268	2	−20	−22	−4.9	31-05-10	2.01	0.06	8	1.3	0.35	12.8	0.5	35.5	0.8
28CP0268	3	−30	−32	−4.8	23-03-11	0.95	0.03	12	1.2	0.35	15.6	0.5	50.8	0.8
28CP0268	4	−40	−42	−4.7	23-03-11	0.84	0.03	6	0.84	0.34	9.8	0.5	45.2	1.0
28CP0268	5	−52	−54	−4.8	31-05-10	0.01	0.01							

[a]Apparent $^3H/^3He$ age = $\ln(1 + {}^3He_{trit}/{}^3H)/\lambda$

Table 2. (continued)

Model		UA				CE					PR					ED				DD			
Parameters		2				3					3					2				2			
Degrees of Freedom		2				1					1					2				2			
Number of Accepted Fits		11				0					1					4				2			
ID	Screen	Temp	EA	χ^2	Pχ^2 (%)	Temp	EA	F	χ^2	Pχ^2 (%)	Temp	EA	R	χ^2	Pχ^2 (″)	Temp	V	χ^2	Pχ^2 (%)	Temp	B	χ^2	Pχ^2 (%)
28CA3309	2																						
28CA3309	3	**9.2**	**2.1**	**0.4**	**81**	9.8	11.7	0.7	0.1	81	10.05	6.6	2.1	0.0	91	7.3	0.0	57.9	0	7.3	0.0	57.9	0
28CA3309	4	**10.2**	**2.4**	**3.0**	**22**	12.3	41.8	0.8	0.1	76	13.05	22.4	4.0	0.0	89	8.1	0.0	76.0	0	8.1	0.0	76.0	0
28CA3336	2																						
28CA3336	3	15.4	0.0	196.6	0	15.4	0.0	0.0	196.6	0	15.41	0.0	0.0	196.6	0	**10.8**	**3.5**	**1.2**	**55**	8.0	0.7	2.1	34
28CA3336	4	6.5	0.0	87.8	0	6.5	0.0	0.0	87.8	0	6.50	0.0	0.0	87.8	0	**4.0**	**2.4**	**6.3**	**4**	2.5	0.5	9.9	1
28CP0168	2	**8.7**	**0.2**	**1.3**	**51**	9.4	424.4	1.0	1.2	27	12.54	81.5	9.3	0.1	75	8.5	0.0	2.1	35	8.5	0.0	2.1	35
28CP0196	1																						
28CP0196	3																						
28CP0207	1																						
28CP0207	3																						
28CP0245	1	**4.1**	**2.7**	**5.8**	**6**	11.3	874.3	0.8	0.5	46	8.24	45.7	5.2	0.1	79	2.2	0.0	84.2	0	2.2	0.0	84.2	0
28CP0245	2	4.5	1.4	10.8	0	8.3	864.3	0.9	8.9	0	**17.11**	**265.0**	**8.6**	**2.4**	**11.8**	3.4	0.0	34.4	0	3.4	0.0	34.4	0
28CP0245	3	**6.5**	**0.7**	**0.1**	**96**	6.7	14.7	0.9	0.0	94	6.83	3.1	2.8	0.0	99	5.8	0.0	6.9	3	5.8	0.0	6.9	3
28CP0248	1	11.0	0.0	4.3	12	11.0	0.0	0.0	4.3	4	11.02	0.0	0.0	4.3	4	11.0	0.0	4.3	12	**10.6**	**0.0**	**3.5**	**17**
28CP0248	2	20.3	0.0	655.8	0	20.3	0.0	0.0	655.8	0	20.32	0.0	0.0	655.8	0	11.1	6.2	23.0	0	6.4	1.5	35.5	0
28CP0248	3	34.6	0.0	1952.0	0	34.6	0.0	0.0	1952.0	0	34.63	0.0	0.0	1952.0	0	**7.6**	**12.9**	**0.4**	**82**	2.0	3.8	19.0	0
28CP0250	1	9.6	0.0	91.7	0	9.6	0.0	0.0	91.7	0	9.64	0.0	0.0	91.7	0	11.0	1.4	49.4	0	**5.1**	**0.5**	**2.5**	**28**
28CP0250	2	9.9	0.0	14.7	0	9.9	0.0	0.0	14.7	0	9.86	0.0	0.0	14.7	0	**8.8**	**0.9**	**0.8**	**67**	8.0	0.2	0.8	66
28CP0250	3	10.3	1.1	22.1	0	10.7	12.6	0.8	21.8	0	10.29	1.2	0.1	22.1	0	9.1	0.0	41.2	0	9.1	0.0	41.2	0
28CP0267	1	**10.6**	**2.0**	**0.6**	**73**	10.7	2.4	0.2	0.6	43	10.84	2.8	0.7	0.6	44	8.8	0.0	50.3	0	8.8	0.0	50.3	0
28CP0267	2	**4.3**	**3.0**	**5.6**	**6**	6.1	38.9	0.7	2.7	10	8.11	40.4	4.8	1.1	29	2.2	0.0	97.6	0	2.2	0.0	97.6	0
28CP0267	3	**9.4**	**1.9**	**0.5**	**79**	9.8	9.0	0.7	0.3	59	10.16	5.6	2.0	0.2	65	7.7	0.0	47.5	0	7.7	0.0	47.5	0
28CP0267	4	1.2	4.7	26.3	0	4.7	66.9	0.6	11.9	0	4.14	31.0	3.5	17.8	0	0.0	0.0	220.9	0	0.0	0.0	220.9	0
28CP0267	5																						
28CP0268	1	11.4	3.0	14.2	0	13.1	25.8	0.7	11.2	0	12.57	8.7	2.0	13.0	0	8.8	0.0	117.1	0	8.8	0.0	117.1	0
28CP0268	2	**7.5**	**0.7**	**2.4**	**30**	9.1	220.0	0.9	0.8	37	10.91	50.7	7.4	0.0	83	6.8	0.0	9.3	1	6.8	0.0	9.3	1
28CP0268	3	**8.8**	**1.2**	**2.3**	**32**	9.2	13.4	0.8	2.1	15	9.05	2.4	1.3	2.2	13	7.7	0.0	22.8	0	7.7	0.0	22.8	0
28CP0268	4	**10.4**	**0.7**	**3.3**	**19**	10.8	19.8	0.9	3.1	8	10.55	1.5	1.4	3.3	7	9.7	0.0	10.6	0	9.7	0.0	10.6	0
28CP0268	5																						
all screens				36.1	5.4				20.3	6.1				10.2	60.2			62.4	0.0			37.9	3.6

degassing (DD) [*Brennwald et al*., 2005]), by minimizing the uncertainty-weighted squared deviations between modeled and measured concentrations [*Aeschbach-Hertig et al*., 1999; *Ballentine and Hall*, 1999], denoted by χ^2 (equation (2)), using a bound constrained quasi-Newton method [*Byrd et al*., 1995].

$$\chi^2=\sum_i \frac{(C_{i,o}-C_{i,m})^2}{\sigma_i^2}(i=\mathrm{Ne},\mathrm{Ar},\mathrm{Kr},\mathrm{Xe}) \tag{2}$$

[21] $C_{i,m}$ are the modeled noble gas concentrations, $C_{i,o}$ and σ^2_i are the observed noble gas concentrations and their uncertainties.

[22] The expected value of χ^2 is the number of degrees of freedom, i.e., the number of measurements less the number of parameters. The probability of the fit for each sample was obtained from the χ^2 distribution with a given number of degrees of freedom (greater than zero) [*Johnson et al*., 1995]. To evaluate the ability of each excess air or degassing model to describe the observed noble gases in the entire data set, the χ^2 contributions of samples were summed and the χ^2 probability was derived, given the total number of degrees of freedom for the entire set [*Aeschbach-Hertig et al*., 1999]. For this evaluation, the data set was split between excess air ($\Delta\mathrm{Ne} > 0\%$) and degassed samples ($\Delta\mathrm{Ne} < 0\%$) and samples without an acceptable fit to any of the models were excluded.

[23] The helium and neon isotope measurements collected from the pumped production wells do not provide sufficient information to estimate excess air fractionation. Therefore, tritiogenic ^{3}He and radiogenic ^{4}He [*Solomon et al*., 1996] were calculated based on the median noble gas recharge temperature and the unfractionated excess air or equilibrium degassing model. This ensured that all data was treated equally. Tritiogenic ^{3}He in degassed samples was calculated assuming equilibrium degassing [*Visser et al*., 2007]. The analytical uncertainty was propagated numerically through the calculations of tritiogenic ^{3}He, radiogenic ^{4}He and the ^{3}H/^{3}He age, by adding 1000 different random realizations of measurement noise to the measured values. The derived parameters were calculated from each realization and the uncertainty was calculated as the standard deviation of the set of 1000 realizations [*Visser et al*., 2007].

2.3.2. Age Models

[24] To derive a groundwater age distribution from the available age tracer data, a shape-free discrete groundwater age distribution model was applied. In this approach, the groundwater age distribution is described by a histogram of n bins of width w with a uniform age distribution within each bin, and is defined by $n-1$ parameters b_i prescribing the fraction of groundwater in each bin. The groundwater age distribution g_t follows equation (3):

$$g_t=\begin{cases} b_i/w & (i-1)w < t \le iw \\ 1-\sum_{i=1}^{n-1} b_i & t > (n-1)w \end{cases} \tag{3}$$

[25] Because most groundwater age tracers (tritium, tritiogenic ^{3}He, ^{85}Kr, SF_6, CFCs) relate to the period since 1950, 1 bin represents groundwater that recharged before 1950. The groundwater age distribution of the old groundwater bin can only be refined if multiple old groundwater tracers (^{39}Ar, radiocarbon (^{14}C), radiogenic ^{4}He) are available.

[26] In this study, we fitted age histograms with 3, 4, 5, and 9 bins to the observed tracer data. Estimating a groundwater age distribution with many more bins (parameters) than tracers is a highly underdetermined problem. For the 9-bin age distribution, an additional constraint was added to the objective function to encourage the smoothness of the estimated groundwater age distribution. The constraint was defined as the sum of the squared differences between the relative proportions (f) of the n adjacent bins and added to the χ^2 contributions of the tracers (equation (4)).

$$S=\sum_i^{n-1}(f_i-f_{i+1})^2 \tag{4}$$

[27] This smoothness constraint is a simplified form of regularization [*Tikhonov and Arsenin*, 1977], similar to the formal shape constraint of the free age distribution described by *Cirpka et al*. [2007].

[28] The groundwater age distributions g_t were also approximated by various combinations of mathematical models [*Maloszewski and Zuber*, 1982], such as the exponential model (equation (5)) defined by a mean travel time τ, the dispersion model (equation (6)) defined by a mean travel time τ and dispersion parameter P_D, and binary mixtures of these two models with a fraction of premodern groundwater (equations (7) and (8)).

$$g_t = e^{-t/\tau}/\tau \tag{5}$$

$$g_t=\frac{e^{\frac{-(t-\tau)^2}{(4P_D\tau\cdot t)}}}{t\cdot\sqrt{(4\pi P_D t/\tau)}} \tag{6}$$

$$g_t=\begin{cases} (1-f_{\mathrm{old}})e^{-t/\tau}/\tau & t\neq\tau_{\mathrm{old}} \\ f_{\mathrm{old}} & t=\tau_{\mathrm{old}} \end{cases} \tag{7}$$

$$g_t=\begin{cases} (1-f_{\mathrm{old}})\dfrac{e^{\frac{-(t-\tau)^2}{(4P_D\tau\cdot t)}}}{t\cdot\sqrt{(4\pi P_D t/\tau)}} & t\neq\tau_{\mathrm{old}} \\ f_{\mathrm{old}} & t=\tau_{\mathrm{old}} \end{cases} \tag{8}$$

[29] In this paper, the derived groundwater age distributions are plotted cumulatively. Ordinary groundwater age distributions (Figure 2a) show the contribution of each age (in years). Cumulative age distributions (Figure 2b) show the fraction of water that is younger than a particular age. The cumulative age distribution has the advantage that it is easier to estimate a fraction of water within a certain age range.

[30] Tritium concentrations in historical precipitation at the Holten well field were reconstructed from seven time series of the Global Network of Isotopes in Precipitation (GNIP: Ottawa, Vienna, and nearby stations Groningen, Emmerich, Beek, De Bilt, and Bad Salzuflen) [*IAEA/WMO*, 2010]. First, the Vienna time series was reconstructed by linear regression with the Ottawa time series for the period prior to 1963. Second, the slopes of regression lines between the five nearby stations to the Vienna time

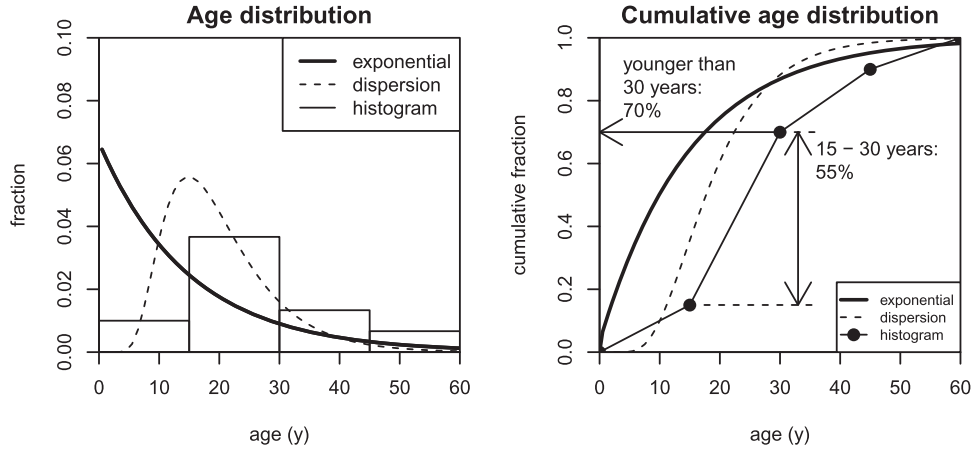

Figure 2. Examples of groundwater age distributions derived from an exponential model ($\tau = 15$ year), a dispersion model ($\tau = 20$ year, $P_D = 0.1$), and a histogram model, (a) plotted directly and (b) cumulatively. The fraction of water within a particular age range is easily interpreted from the cumulative age distribution.

series were determined. The average of the slopes, weighted by the inverse distance to the Holten well field, was then used to reconstruct the local historical tritium concentrations in precipitation. The historical tritium concentrations were compared with the sum of tritium and tritiogenic ^{3}He concentrations ("initial tritium") observed in the monitoring wells, assuming piston flow toward the short screened monitoring wells. This comparison was aimed at verifying the historical concentrations of tritium in precipitation, as well as estimating the escape of tritiogenic ^{3}He to the atmosphere during transport in the unsaturated zone. Historical concentrations of tritium in precipitation have also been verified in short screened monitoring wells in sandy regions of the Netherlands [*Meinardi*, 1994].

[31] The time series of the ^{85}Kr activity in the atmosphere collected and measured at Freiburg im Breisgau (Institute of Atmospheric Research (IAR), Freiburg, Germany) was used for Holten without correction. This is likely a lower estimate for our study area because of the proximity to the reprocessing facilities Sellafield and La Hague compared to Freiburg [*Winger et al*., 2005].

3. Results

3.1. Monitoring Well Results

3.1.1. Dissolved Gas Results

[32] The noble gas concentrations from the diffusion samplers—except helium—were fitted to all of the excess air (UA, CE, PR) and degassing (ED, DD) models (Table 2). Of the 15 samples containing excess air ($0\% < \Delta Ne < 50\%$), 11 samples fitted to the unfractionated air model with a probability of more than 5%. One sample fitted only to the partial reequilibration model. Three samples did not give a probable fit to any of the excess air models. Of the seven samples that showed signs of degassing ($-52\% < \Delta Ne < 0$), four fitted to the equilibrium degassing model and two fitted to the diffusive degassing model. For the entire set of samples containing excess air, the partial reequilibration model is the most appropriate, with a combined probability of 60%. Both the unfractionated air model (5.4%) and closed equilibrium model (6.1%) are acceptable. Neither the equilibrium degassing or diffusive degassing model are acceptable for all degassed samples because some samples specifically fit to one model, yielding a very high χ^2 to the other model. In summary, no single excess air or degassing model appears to be capable of describing all the observed noble gas concentrations in this data set. The median estimated recharge temperature of the accepted fits (10.1°C) is in good agreement with the mean annual air temperature (9.6°C) recorded at the nearby Twenthe meteorological station [*KNMI*, 2012].

[33] All samples contained excess dissolved nitrogen with respect to the dissolved argon concentration (Figure 3), which is the result of denitrification. The total dissolved gas pressure measured in the diffusion samplers correlated with the nitrogen concentration ($R^2 = 0.98$) indicating that the gas source and the cause of degassing is denitrification [*Visser et al*., 2007, 2009d]. The total dissolved gas pressure was measured both in the field and in the diffusion

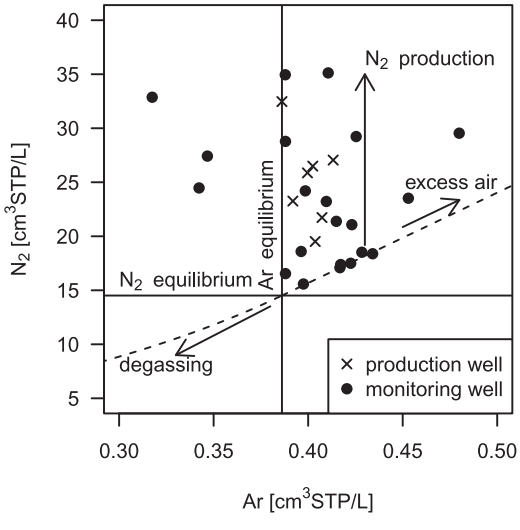

Figure 3. Argon and nitrogen concentrations in production and monitoring wells show excess nitrogen from denitrification.

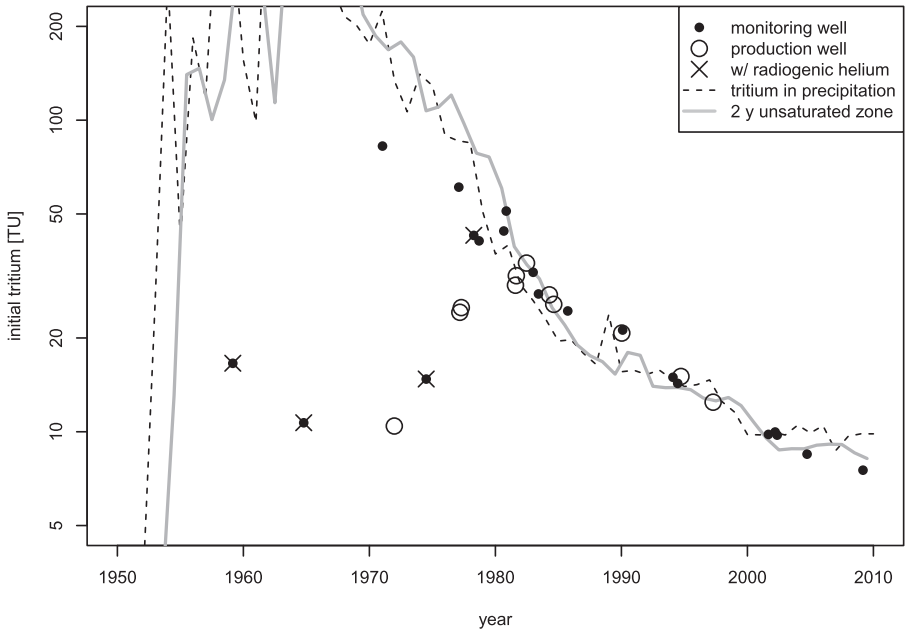

Figure 4. Historical tritium concentrations in precipitation after a 2 year unsaturated zone travel time. Sum of tritium and tritiogenic ^{3}He in samples is plotted at the ^{3}H/^{3}He recharge year.

sampler. These measurements correlated ($R^2 = 95\%$) indicating that field probe total dissolved gas measurements can serve as proxy for dissolved nitrogen concentrations.

3.1.2. Initial Tritium Concentrations in Monitoring Well Samples

[34] "Initial tritium" refers to the tritium concentration which entered the saturated zone at the time of recharge. Under the assumption of piston-flow conditions, it is the sum of tritium and tritiogenic ^{3}He in the sample. Three samples from monitoring wells contain less than 0.05 ($\pm$0.02) TU tritium and can be considered more than 99% premodern. The available noble gas data for one of these samples contained 6.8×10^{-7} cm^3 STP/L radiogenic ^{4}He. Assuming a radiogenic helium isotope ratio of 2×10^{-8}, 1.36×10^{-14} cm^3 STP/L of ^{3}He can be attributed to radiogenic helium, less than 0.2% of the measured concentration of ^{3}He (7.53×10^{-12} cm^3 STP/L). The remainder was considered tritiogenic and the initial premodern tritium concentration was calculated to be 3.0 ($\pm$0.4) TU. This concentration was used for tritium in precipitation prior to 1953. This estimate is less than the 5 TU reported for central Europe by *Roether* [1967].

[35] For all other samples, the ^{3}H/^{3}He ages were calculated, and the sum of tritium and tritiogenic ^{3}He (initial tritium) was plotted together with the reconstructed concentrations of tritium in historical precipitation (Figure 4). Groundwater samples with a ^{3}H/^{3}He age of less than 10 years contain less tritium than present day annual mean precipitation, indicating a loss of tritiogenic ^{3}He from tritium decay in the unsaturated zone or preferential recharge during winter periods. For screens younger than 30 years, the sum of tritium and tritiogenic ^{3}He in samples from the monitoring network is consistent with the reconstructed tritium concentrations in historical precipitation, considering a 2 year unsaturated zone travel time.

[36] Seven monitoring well samples with a ^{3}H/^{3}He age of more than 30 years (recharged before 1980) show larger discrepancies with the reconstructed historical concentrations of tritium in precipitation, possibly caused by dispersion or binary mixing with a fraction of old water. A small fraction of radiogenic ^{4}He confirms an old groundwater component in four of these screens. This is in agreement with field tests and theoretical expectations [*Engesgaard et al*., 1996; *Gelhar et al*., 1992]. The ^{3}H/^{3}He ages of samples that show dispersion or mixing may differ from the mean or median ages of the actual age distribution of the sampled groundwater and are likely biased toward recharge periods with high concentrations of tritium in precipitation, i.e., the bomb-peak period. The effects of dual domain mass transfer are not sufficient to explain these large differences of tritium concentrations [*Neumann et al*., 2008].

3.1.3. Vertical Age Profiles

[37] At the monitoring well locations, the surface elevation varies between 15 and 21 m above mean sea level (msl). Groundwater levels in the monitoring wells varied between 10.7 and 13.6 m msl at the time of sampling. ^{3}H/^{3}He ages generally increase with depth in the top 30 m, ranging from less than 1 to 31 years (Figure 5). A downward vertical groundwater velocity of 0.8–1 m/yr was estimated by dividing the depth of the sampled screen by the ^{3}H/^{3}He ages of samples that did not show significant dispersion or mixing with premodern groundwater (i.e., for which initial tritium follows the historical input concentrations).

[38] All groundwater samples below -10 m msl contain either a mixture of young and old groundwater or exclusively old groundwater. Three deep monitoring wells below -25 m msl contain less than 0.03 ($\pm$0.02) TU tritium, indicating the depth of the boundary between modern and "old" groundwater.

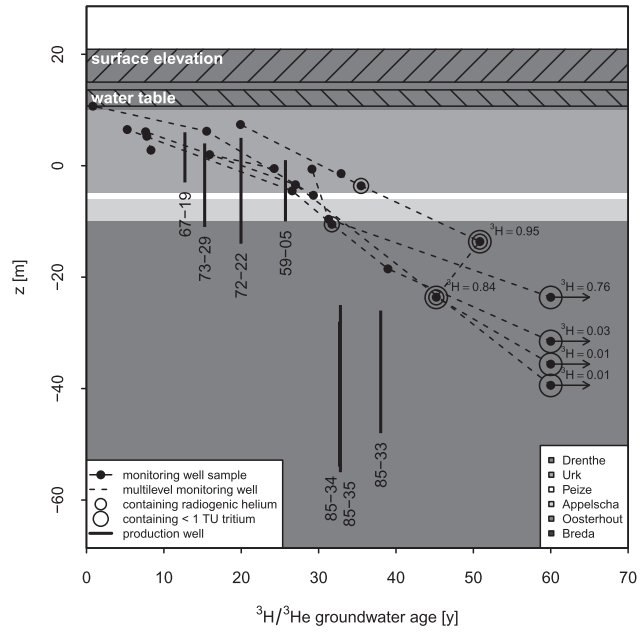

Figure 5. Vertical profile of ^{3}H/^{3}He groundwater ages in production wells and multilevel monitoring wells (screens from the same well are connected by dashed lines). Screen lengths are indicated by vertical lines, age uncertainty by horizontal error bars for the monitoring screens.

3.2. Production Well Results

[39] In this section, first the measured tracer data from the production wells are reported and apparent ages for each of the separate tracers are derived. Second, a combined qualitative age tracer interpretation is presented. Third, the measured tracer concentrations are used to estimate groundwater age histograms using a novel discrete approach as well as commonly used mathematical models.

[40] All samples collected from the production wells contained more than 1 TU of tritium, indicating that all wells contain a significant fraction of modern groundwater and are therefore vulnerable to recent anthropogenic contamination. All samples contained detectable amounts of ^{85}Kr, confirming the young groundwater detected by tritium. The presence of tritium in deep production wells, in contrast to monitoring wells at the same depth, indicates that they draw a fraction of younger groundwater from shallower parts of the aquifer.

[41] Neon concentrations in the production wells vary from moderate amounts of excess air (n = 8) to slight depletion due to degassing by in-aquifer nitrogen production (n = 3). Depleted neon concentrations are found in production wells at the southern half of the well field, close to the monitoring wells under agricultural land use in which depleted neon concentrations were detected. The tritiogenic ^{3}He component in these samples was calculated assuming degassing at the time of recharge, which yields a lower estimate than assuming degassing at the time of sampling [*Sültenfuß et al*., 2011; *Visser et al*., 2007]. The ^{85}Kr and ^{39}Ar isotope ratios are not affected by degassing and do not require a correction.

[42] The relative abundances of nitrogen and argon (measured in the extracted gas for ^{85}Kr and ^{39}Ar determination) were converted to dissolved gas concentrations using the measured neon concentrations, assuming unfractionated excess air. This calculation also assumes the gas extraction efficiency of neon, argon, and nitrogen is equal. The resulting figure (Figure 3) shows the enrichment of nitrogen with respect to argon. The calculated excess nitrogen from denitrification is equivalent to 20–100 mg/L nitrate. Shallow production wells contain both 2–6 mg/L dissolved oxygen and excess nitrogen by denitrification, indicating these wells pump a mixture of oxic and anoxic groundwater. Dissolved oxygen is absent in the deep production wells.

[43] Tritiogenic ^{3}He concentrations range from the equivalent of 6.4 TU in one of the deep production wells to the equivalent of 27 TU in one of the shallow production wells. The deep production well samples also contain a radiogenic ^{4}He component of 10–24% of atmospheric equilibrium ^{4}He concentrations.

[44] Vertical profiles of isotopes measured in the shallow production well 67-19 and in the monitoring wells in the casing of the nearby deep production well 85-35 provide additional insight in the flow structure and mixing around these wells (Figure 6). The measured tritium (Figure 6a) and tritiogenic ^{3}He (Figure 6b) concentrations in the shallow monitoring well in the casing of 85-35, at 26 m well

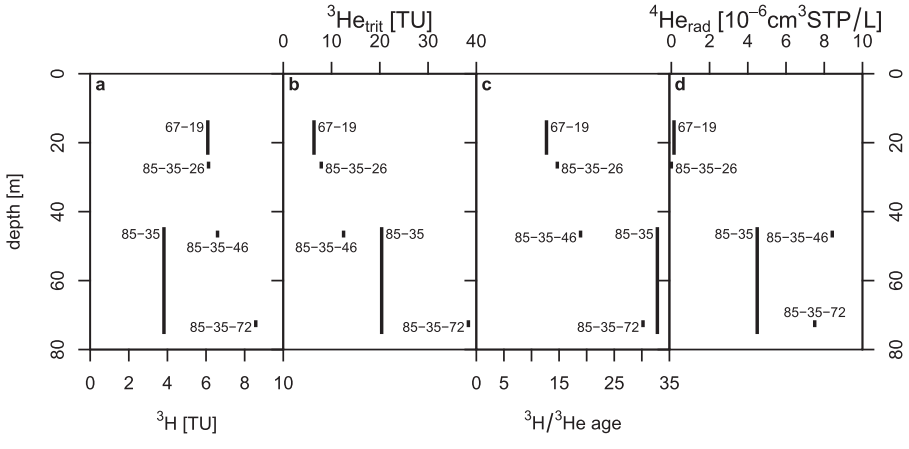

Figure 6. (a) Profiles of tritium, (b) tritiogenic ^{3}He, (c) ^{3}H/^{3}He age, and (d) radiogenic ^{4}He in nearby production wells 67-19 and 85-35, and the monitoring wells in the casing of 85-35.

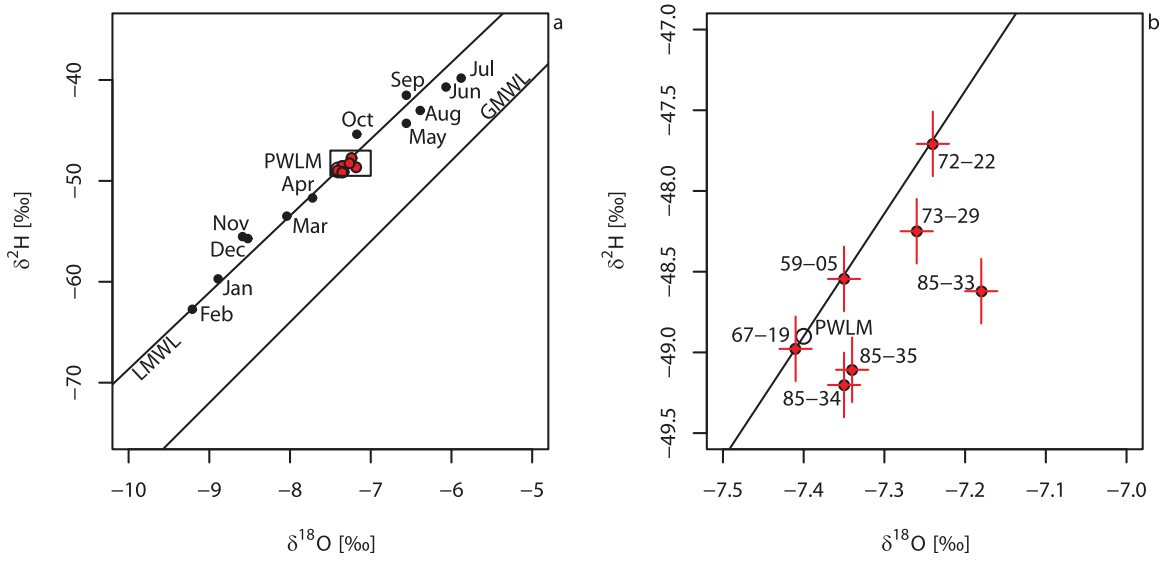

Figure 7. Stable isotopes of water in production well samples (red). (a) The annual precipitation-weighted local mean (PWLM, open circle) and monthly mean values of the Groningen GNIP station [*IAEA/WMO*, 2010] are also plotted, together with the global (GMWL) and local (LMWL) meteoric water line. (b) Deep production wells show a significant enrichment in ^{18}O.

above the production screen, correspond well to those measured in production well 67-19. Tritium concentrations increase along the screen of the deep production well. The mixture pumped by the deep production well contains less tritium indicating an old groundwater component is mixed in with the tritium bearing young groundwater. On the other hand, the measured radiogenic ^{4}He component (Figure 6d) in the two deeper monitoring screens (85-35-46 and 85-35-72) is higher than in the production well 85-35, indicating a larger fraction of young groundwater is present in the production well than in these monitoring wells [*Sültenfuß et al*., 2011]. These discrepancies are likely the result of lateral variations of groundwater inflow sources at the same depth of the production well screen.

[45] The ^{39}Ar activities in the shallow production wells are all over 90 (±10) percent of the modern atmospheric activities (%modern), while the ^{39}Ar activities of the three deep production wells range from 77 to 51 (±8) %modern. These ^{39}Ar activities found in the deep production wells correspond to ages of 100 (±40) years to 260 (±60) years. Given the presence of tritium in all these samples, the actual age distribution of groundwater in these wells ranges from present to possibly several hundreds of years, depending on the fraction of old groundwater bearing the low ^{39}Ar activities. The ^{39}Ar activities indicate a groundwater system with mean ages in the centennial rather than millennial scale.

[46] Stable isotopes of water (^{2}H and ^{18}O) measured in the production wells show a clear distinction between the shallow and deep wells (Figure 7). Stable isotopes in shallow wells are close to the present meteoric water line, while the deep wells show a significant enrichment in ^{18}O indicative of an evaporation signal. This could indicate soil evaporation from barren sand on the Holterberg before forestation. The isotope ratios of the groundwater samples are very close to the precipitation-weighted local mean (PWLM) isotope ratios, indicating that there is no preferential recharge of winter precipitation that would bias the tritium input into the groundwater system, which is in agreement with previous observations [*Gehrels et al*., 1998]. The isotope signatures in the wells are slightly shifted toward the mean monthly isotope ratios between May and October. This shift would indicate an unusual preference for recharge of summer precipitation.

[47] The radiogenic ^{4}He concentrations correlate with the ^{39}Ar activities in the three production wells (Figure 8a), either as a result of mixing between young and old groundwater or by the release of ^{4}He on the ^{39}Ar decay time scale. A ^{4}He release rate (R) between 10 and 20 $\mu cm^3\ m^{-3}\ yr^{-1}$ would yield the observed ^{4}He concentration and ^{39}Ar activities. This rate is 1 order of magnitude smaller than the in situ ^{4}He release rates reported by Solomon [*Solomon et al*., 1996] and less than the 50 $\mu cm^3\ m^{-3}\ yr^{-1}$ found near the Ems [*Sültenfuß et al*., 2011]. However, with such accumulation rates, ^{4}He should also be visible in the monitoring wells at the $^{3}H/^{3}He$ time scale (Figure 8b) which was not observed. Consequently, the radiogenic ^{4}He in the deeper wells is either the result of a diffusive external influx of ^{4}He from the underlying Tertiary marine sediments that form the hydrological base of the aquifer (Breda Formation) or it indicates a groundwater component with an age of several thousands of years that has accumulated ^{4}He in situ. Additional tracer information such as radiocarbon (^{14}C) [*Fontes and Garnier*, 1979; *Kalin*, 1999; *Mook*, 1980] is required to test these hypotheses.

[48] The $^{3}H/^{3}He$ ages in the shallow production wells vary from 13 to 28 years, those in the deep production wells from 33 to 38 years. These $^{3}H/^{3}He$ ages in mixed samples are biased toward recharge periods with high concentrations of tritium in precipitation. The concentrations

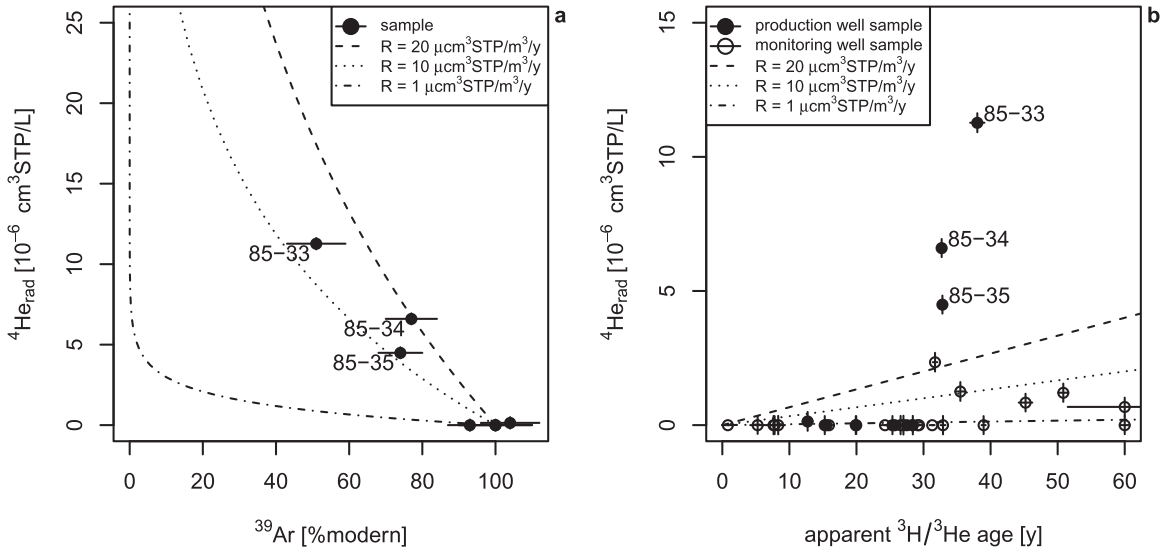

Figure 8. (a) Radiogenic ^{4}He and ^{39}Ar in production well samples. (b) Radiogenic ^{4}He against ^{3}H/^{3}He age in production and monitoring well samples. Dashed lines show the accumulation of radiogenic ^{4}He on the ^{39}Ar and ^{3}H/^{3}He time scales assuming different production rates.

of tritium and tritiogenic ^{3}He in the shallow production wells are similar to those found in the monitoring wells (Figure 4). The ^{85}Kr ages range from 12 to 13 years in the shallow production wells to 27–39 years in the deep production wells. Like ^{3}H/^{3}He ages, ^{85}Kr ages are biased toward the period with the higher initial tracer concentration. ^{85}Kr ages are younger than the ^{3}H/^{3}He ages (Table 1), indicating that the production wells sample a mixture of water with young groundwater ages.

[49] Tracer-tracer plots (Figure 9) combine the measured tracer concentrations in the production well samples with the decay-corrected predicted tracer concentrations for various models and travel times. The piston-flow model (black line) still shows the annual variations in ^{85}Kr, tritium and tritiogenic ^{3}He concentrations. The mixing of groundwater ages in the exponential model (bold grey line) results in a smooth line distinctly different from the piston-flow model.

[50] Deriving a discrete groundwater age distribution is essentially estimating mixing fractions of end-members representing the average tracer concentration for each groundwater age bin of the histogram [*De Louw et al*., 2011]. The tracer-tracer plots are illustrative of the end-member mixing character of the discrete groundwater age distribution model. The four end-members of the 4-bin groundwater age distribution are calculated by taking the average of the decay-corrected tracer concentrations within the 20 year bins (large black dots in all plots of Figure 9 numbered 1–4). For example, the first point represents the average decay-corrected tracer concentrations for groundwater with an age between 0 and 20 years. Bold dashed lines connect adjacent end-members; thin dashed lines connect the first two end-members with the old fraction end-member.

[51] The values of the end-members need to be known, to be included in the estimating of the mixing ratios. Since none of the wells that were sampled for ^{39}Ar produces exclusively old groundwater (all wells contain tritium) it is not possible to directly define an ^{39}Ar activity representative of the old groundwater component in the mixture. The ^{39}Ar end-member of the old fraction was therefore estimated to be 45% modern (representing an age of 310 years), based on the plots of ^{39}Ar versus tritium and ^{85}Kr.

[52] All samples fall within the triangle of end-members 1, 2, and 4, and appear to be mixtures between the first (0–20 years), second (20–40 years), and fourth (>60 years) end-member of the 4-bin age distribution. The presence of a small component of the third bin cannot be excluded, but none of the samples appear to be dominated by this bin. The apparent absence of groundwater from the third bin (40–60 year) is consistent with the observation that all samples from monitoring wells in this age range show mixing with premodern groundwater.

[53] Production well 59-05 falls outside the end-member mixing triangle for tritiogenic ^{3}He and ^{85}Kr (Figure 9d), and appears to contain some excess tritiogenic ^{3}He. The measured neon concentration in this sample was below equilibrium indicating degassing of noble gases. The enrichment of tritiogenic ^{3}He in this sample may be attributed to a trapped gas phase in the aquifer containing legacy tritiogenic ^{3}He from the bomb pulse. This effect has been shown to occur in two-phase flow and transport simulations of degassing by denitrification [*Visser et al*., 2009d]. The effect on the ^{85}Kr has not been simulated. Given the input curve of ^{85}Kr, the effect of a trapped gas phase would be the net release of krypton with a lower ^{85}Kr activity. Due to the higher solubility of krypton, this effect would be 1 order of magnitude smaller than for tritiogenic ^{3}He.

3.3. Groundwater Age Distributions in Production Wells

[54] Discrete age distributions were quantified by minimizing the χ^2 deviations between measured and modeled

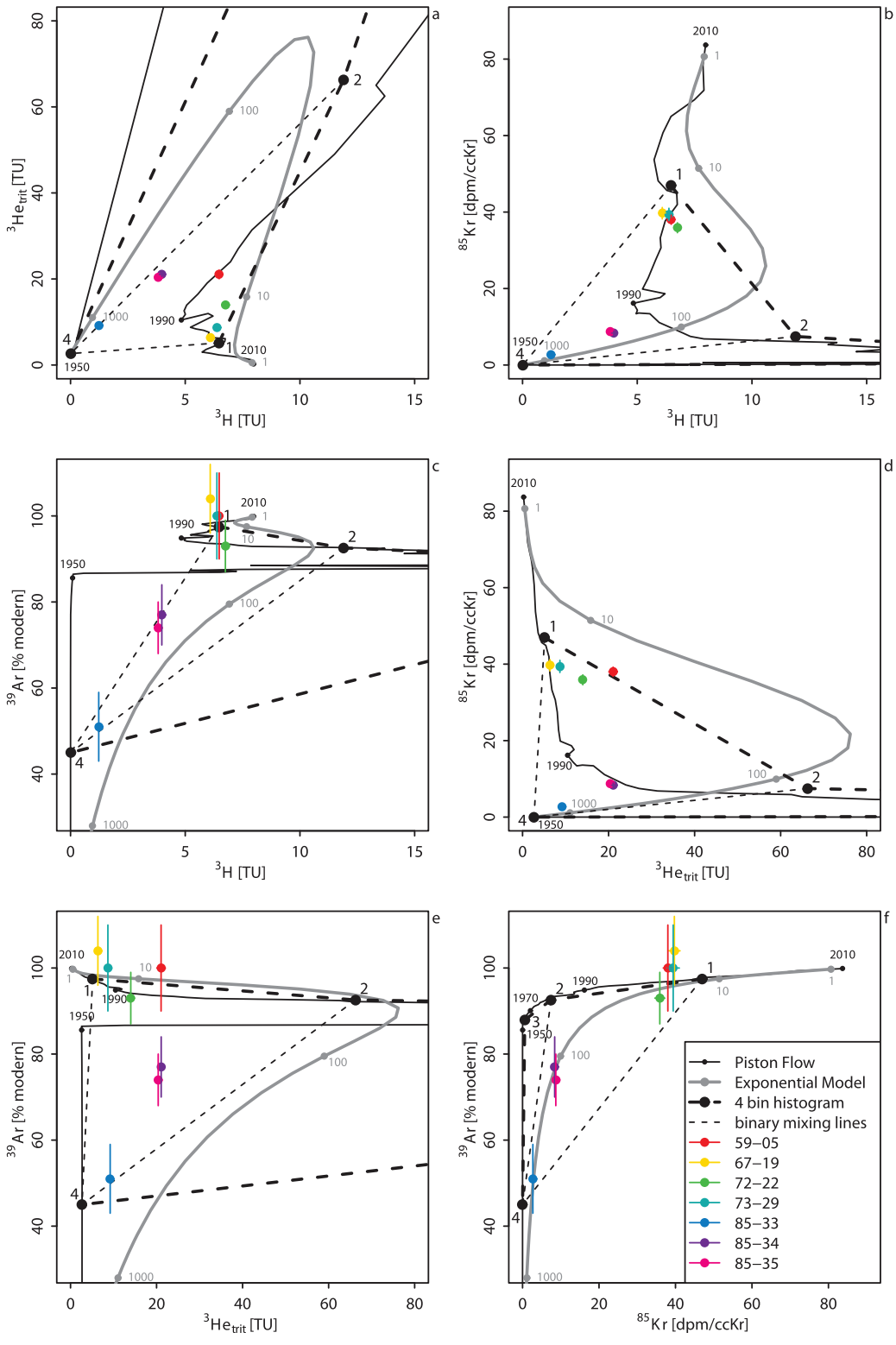

Figure 9. Plots of all combinations of measured tracers with the predicted tracer concentrations for the piston flow and exponential model, and the end-members of the 4-bin discrete age distributions. Piston flow recharge years are indicated by small black numbers, mean travel times of the exponential model by small gray numbers, the bin numbers of the 4-bin discrete age distribution by large blank numbers. The third bin end-member is outside the plotted scale in most of the graphs.

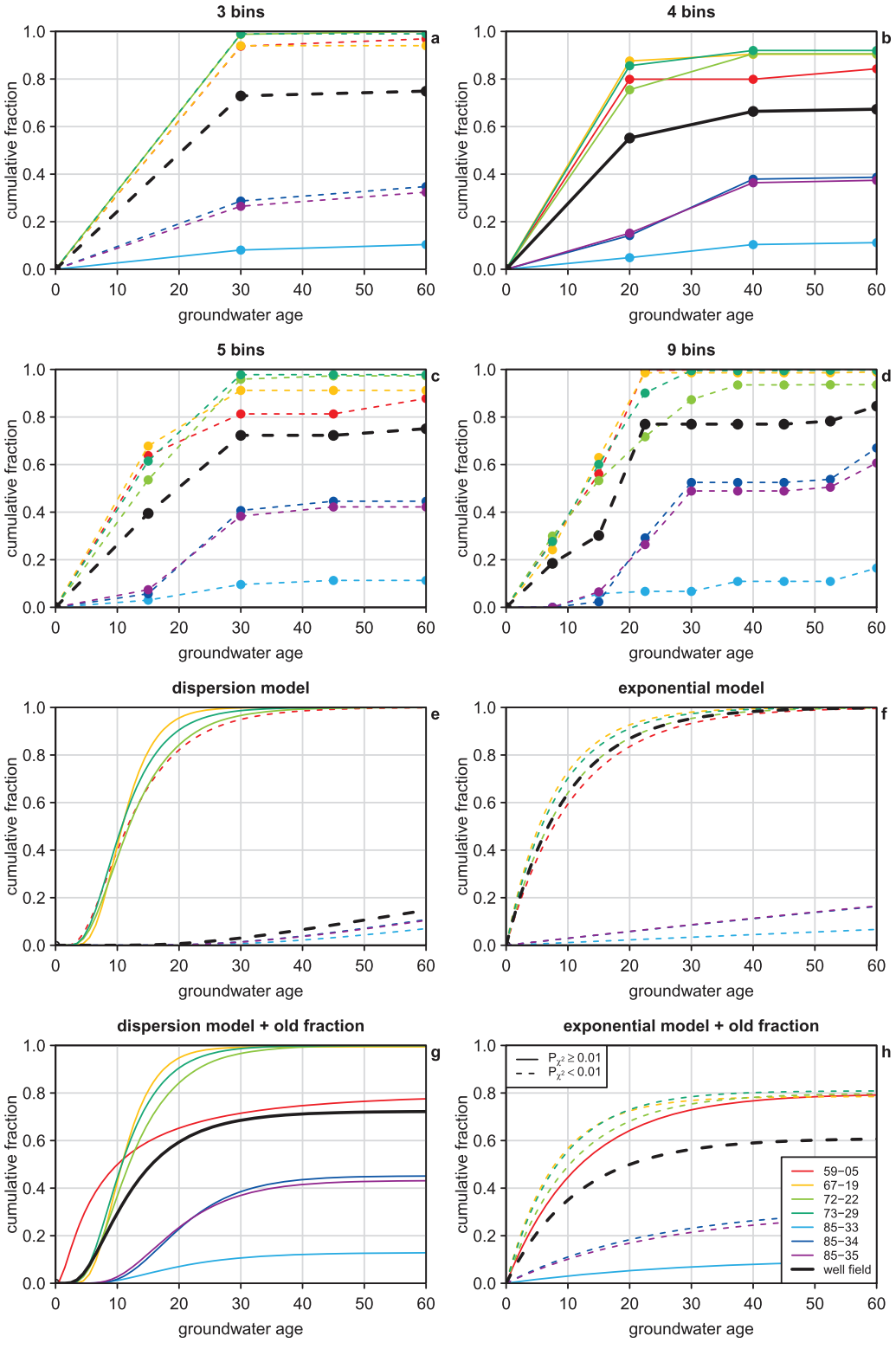

Figure 10. Cumulative groundwater age distributions of the individual production wells and the well field as a whole (equation (1)) described by discrete models with (a) 3, (b) 4, (c) 5, and (d) 9 bins, (e) a dispersion model, (f) an exponential model, (g) a dispersion model with an old fraction, (h) an exponential model with an old fraction. Accepted models ($P\chi^2 \geq 1\%$) are solid lines, rejected models ($P\chi^2 < 1\%$) are dashed lines.

tracer concentrations. The modeled concentrations were calculated by multiplying the fraction of water in each bin with the average of the decay-corrected tracer concentrations for each bin. First, a 3-bin groundwater age distribution (two parameters) was fitted (Figure 10a and Table 3). The breaks between these bins are located at 30 and 60 years, corresponding to the recharge years 1980 and 1950. The χ^2 probability of the groundwater age distributions is less than 1% for all production wells, except 72-22 and 85-33 (Table 3). The 3-bin groundwater age distribution appears too restrictive to describe the actual groundwater age distribution with an acceptable probability, yet the shape of the groundwater age distributions is informative.

[55] The shapes of the 4-bin groundwater age distributions (three parameters) are similar to the 3-bin groundwater age distributions (Figure 9b). The fractions of old groundwater in the shallow production wells are estimated to be larger (8–16%), while the young fraction is almost entirely younger than 20 years in these wells. In the deep production wells, the first bin (0–20 years) contributes less than the second bin (20–40 years). The χ^2 probability of these groundwater age distributions vary from 5% to 95%. The high $P\chi^2$ for well 85-33 might indicate that the uncertainty of the tracer data has been underestimated. The combined probability of the 4-bin model is 5%. The 4-bin groundwater age distribution predicted for the entire well field (equation (1)) is in between those of the shallow production wells and deep production wells. For the entire well field, 55% of the pumped groundwater is younger than 20 years, 33% is older than 60 years. Only 11% is 20–40 years old and less than 1% is estimated to be 40–60 years old. The χ^2 probability of this distribution is lower (2%) partly due to the lower propagated measurement uncertainty of the average tracer concentrations.

[56] The 5-bin groundwater age distributions (Figure 9c) reveal more detail and show larger differences between the shallow production wells. No χ^2 probability can be calculated with zero degrees of freedom, but the reduction of the χ^2 error is informative of the improvement of the fit. The reduction of the χ^2 indicates that the 5-bin groundwater age distribution more closely resembles the age tracers produced by these wells. The 9-bin groundwater age distributions (Figure 9d) are similar to the 5-bin groundwater age distributions.

[57] The dispersion model defined by two parameters [*Maloszewski and Zuber*, 1982] estimates probable ($P\chi^2 \geq 64\%$) groundwater age distributions for three of the shallow production wells (Figure 10e and Table 3). A binary mixture of the dispersion model with an old fraction (three parameters, Figure 10g) estimates probable ($P\chi^2 \geq 16\%$) groundwater age distributions for all of the production wells. The mean travel time parameter of the dispersion model for three of the shallow production wells is 12–14 years with a dispersion parameter of 0.07–0.13 and an old fraction of less than 1%. The three deep production wells have a mean travel time parameter of 21–22 years for the young fraction and a dispersion parameter of 0.08–0.12. Two deep wells have an old fraction of 55–57%; the third deep well has an old fraction of 87%. The groundwater age distribution of the entire well field is modeled by the dispersion model with an old fraction of 28% with a χ^2 probability of 10%. This age distribution agrees

Table 3. Results for Groundwater Travel Time Distribution Models in Terms of χ^2 (Equation (1)) and χ^2 Probability ($p\chi^2$)

	3-bin		4-bin		5-bin	9-bin	DM				DM-f_{old}					EM			EM-f_{old}			
Model							2				1					3			2			
Degrees of freedom	2		1		0	−4																
Well	χ^2	$P\chi^2$ (%)	χ^2	$P\chi^2$ (%)	χ^2	χ^2	τ	P_D	χ^2	$P\chi^2$ (%)	τ	P_D	f_{old}	χ^2	$P\chi^2$ (%)	τ	χ^2	$P\chi^2$ (%)	τ	f_{old}	χ^2	$P\chi^2$ (%)
59-05	32.7	0	1.7	19	1.0	213.2	14.2	0.18	30.3	0	13.4	0.88	0.20	1.9	16	11.1	195.4	0	12.2	0.20	2.9	23
67-19	76.8	0	3.9	5	3.8	1.1	12.0	0.06	0.9	63	12.0	0.07	0.01	0.9	35	7.7	204.5	0	7.8	0.21	24.4	0
72-22	1.3	51	0.6	45	0.1	0.0	14.0	0.13	0.4	83	14.0	0.13	0.00	0.4	54	9.8	186.3	0	10.5	0.20	25.3	0
73-29	21.8	0	1.5	22	0.2	0.2	12.5	0.11	0.2	92	12.5	0.11	0.00	0.2	69	8.3	141.4	0	8.6	0.19	18.6	0
85-33	4.7	10	0.0	95	0.0	0.7	4500	9.12	262.1	0	21.8	0.12	0.87	0.0	96	870.4	101.1	0	29.3	0.89	9.2	1
85-34	40.2	0	3.4	6	2.1	0.2	400	0.93	633.7	0	21.9	0.08	0.55	1.9	16	337.4	339.3	0	24.0	0.68	56.3	0
85-35	36.0	0	3.1	8	1.9	0.2	400	0.91	1142.4	0	21.4	0.09	0.57	1.6	20	332.2	564.8	0	24.9	0.69	51.2	0
Well field mixture	12.5	0	5.8	2	1.7	0.4	10000	30.79	8683.9	0	14.2	0.18	0.28	2.7	10	9.8	5431.4	0	11.7	0.39	66.9	0
Degrees of freedom	14		7		0	−28	14				7					21			14			
Total	213.4	0	14.2	5	9.0	215.5			2069.9	0				6.9	44		1732.9	0			187.9	0

well with the 4-bin discrete age distribution, estimating a large fraction (59%) of pumped groundwater that is younger than 20 years and a small fraction (13%) in the 20–40 year old age range. 1% is estimated to be 40–60 years old and 28% is older than 60 years.

[58] The exponential model [*Maloszewski and Zuber*, 1982] provides no plausible age distribution for any of the production wells or for the well field as a whole (Figure 10f and Table 3). A binary mixture of an exponential model with an old component (Figure10h) provides a good fit for only two of the production wells. The contribution of bomb-peak groundwater in the continuous exponential model causes large deviations from the measured tritium and tritiogenic ^{3}He concentrations (see Figure 8a) resulting in high χ^2 values.

4. Discussion

[59] The age distributions of seven production wells of the Holten well field were characterized based on ^{85}Kr, tritium, tritiogenic ^{3}He and ^{39}Ar using a discrete age model and existing mathematical age models. The network of monitoring wells surrounding the well field was investigated using ^{3}H/^{3}He dating to establish the age stratification of the aquifer.

[60] The age depth profile did not show a logarithmic age increase over the entire depth of the aquifer (Hypothesis A). While an age increase with depth was observed in the top 30 m, deeper screened monitoring wells appear to sample groundwater that is strongly affected by dispersion or mixing with "old" groundwater.

[61] If all parts of the aquifer contribute equally to the mixture of groundwater pumped by the production wells, the age distributions of pumped groundwater should reflect the age stratification of the aquifer. The combined age distribution of the entire well field does not fit to an exponential age distribution (Hypothesis B). While this is in agreement with the observation that the age stratification was not logarithmic over the entire depth of the aquifer, a more detailed analysis shows that the Holten well field as a whole does not represent the age stratification in the aquifer. Both the 4-bin discrete age distribution and the dispersion model age distribution with an old fraction predict over 55% of groundwater with an age of less than 20 year in the pumped groundwater mixture of the entire well field. Groundwater in that age range is only found in the top 10–15 m of the aquifer, representing less than 20% of the aquifer thickness. Groundwater in the age range of 20–40 years constitutes 10–15% of the pumped groundwater and 40–60 year old groundwater appears to contribute 1% to the pumped groundwater mixture. Monitoring well results indicated that groundwater in this age range was impacted by dispersion or mixing with old groundwater. Old groundwater (that recharged before 1950) constitutes about 30% of the pumped groundwater. Tritium-dead groundwater is found below −25 m msl, in approximately 50% of the aquifer thickness. This comparison shows that the Holten well field as a whole does not represent the age stratification in the aquifer because it preferentially pumps shallow groundwater from the Urk and Peize Formations which have a higher hydraulic conductivity (Hypothesis B).

[62] The differences between the groundwater age distributions derived for the individual production wells show that these wells influence each other by competing for capture area. The resulting groundwater age distributions of individual production wells is different from the age stratification in the aquifer (Hypothesis C).

[63] The old fraction in the shallow production wells is probably caused by high gradients abstracting water from the Oosterhout Formation in the vicinity of the shallow production wells. The difference between the groundwater age distributions of the deep production wells is likely the result of the influence of shallower production wells in the well field, for example the intermediately deep production well (04-38) near the deep production well 85-33 (Figure 1). The measured concentrations of age tracers in this intermediate production well are in between those of the nearby shallow production wells (59-05 and 72-22) and the deep production well (85-33). The intermediate production well captures shallow and younger groundwater that would have been captured by the deep production well if well 04-38 were absent. In terms of the age distribution, intermediate well 04–38 captures the fraction of modern water that contributes nearly 40% to the other deep production wells (85-34 and 85-35) but not to 85-33.

[64] Mixing of groundwater components with different ages is an important process in production well fields. Our study shows that the resulting age distributions of the production wells can be deconvoluted by the combination of tracers with different decay-corrected historical records, like tritium, ^{3}He and ^{85}Kr. The discrete groundwater age distribution model appears to be a suitable approach to derive an age distribution from tracer concentrations in settings where the age distribution cannot be assumed to follow standard mathematical models for individual wells. A production well field where wells compete for capture area is an example of such a setting.

[65] The benefit of the ^{39}Ar measurements is relatively small for the shallow production wells because of the large fraction of young groundwater in those wells. However, the ^{39}Ar measurements did reveal that the age structure in deeper parts of the aquifer is on a centennial time scale and significantly improved the dating of deep production wells.

[66] The uncertainties of the historical concentrations of ^{85}Kr and tritium in recharging groundwater have not been considered in detail. Tritium and tritiogenic ^{3}He measurements from short screened monitoring wells in combination with the historical tritium input concentration in precipitation were used to derive a travel time through the unsaturated zone of 2 years. Stable isotopes of water in groundwater are close to the precipitation-weighted annual mean and therefore preferential recharge of winter precipitation is not expected to affect the tritium input. If the uncertainties in the input are included, more weight will be assigned to the ^{39}Ar measurements because the initial activity of ^{39}Ar is spatially and temporally better constrained than that of ^{85}Kr and tritium.

[67] Combined tracer methods only add information to the groundwater age distribution if the historical recharge concentrations, the radioactive decay constants or the ingrowth rates are distinctly different [*Larocque et al.*, 2009]. The curve of historical atmospheric concentrations of SF_6 is very similar to the decay-corrected activities of

^{85}Kr in the atmosphere. The sensitivity to excess air, degassing and local sources of contamination add to the uncertainty in the source of SF_6. Additional SF_6 measurements could potentially improve the understanding of structural model errors and observational errors.

[68] The historical atmospheric concentrations of CFCs reach a plateau in the early 1990s. Because this is distinctly different from SF_6 or ^{85}Kr, CFCs could add information about the contribution of 20–30 year old groundwater in the mixture. However, CFCs are very often subject to local contamination and also to degradation in anoxic aquifers [*Hinsby et al*., 2007; *Sebol et al*., 2007; *Tesoriero et al*., 2000; *Visser et al*., 2009d].

[69] Radiocarbon (^{14}C) from the deep production wells could have revealed more details about the age structure of the deeper parts of the aquifer. To further investigate the age structure in the deeper part of the aquifer, ^{39}Ar measurements are needed from monitoring wells that are screened deeper than those currently sampled. Noble gas data from such monitoring wells in combination with ^{39}Ar could map the source, depth and release rate of the radiogenic ^{4}He in the aquifer [*Solomon et al*., 1996].

[70] A Bayesian approach to interpreting the multiage-tracer data sets [*Massoudieh et al*., 2012] in combination with a shape-free age distribution [*Cirpka et al*., 2007] with a formal smoothness constraint will provide flexibility and an uncertainty analysis of the derived age distribution, and can perhaps attribute these uncertainties to model uncertainty (e.g., age tracer input or vadose zone transport) or measurement uncertainty (e.g., analytical and representative capture volume of production wells), directing future efforts to reduce uncertainty of the age distribution.

[71] The Holten drinking water production well field has expanded historically, most significantly by the installation of the deep production wells. While the hydrodynamic conditions (heads) have likely reached a new steady state, the tracer conditions may still be transitioning from a previous steady state (i.e., pumping by shallow production wells only before 1985, or no significant pumping before 1960) to the present day pumping regime [*Zuber et al*., 2011]. Therefore, the derived tracer-based age distributions are valid under the current pumping regime at present, and may evolve further. In addition, future variations of well pumping rates, abandoning of wells or drilling additional wells will impact the groundwater captured by existing wells and therefore also the age distribution of individual wells. Transient numerical flow models are required to predict the response to such changes in the well field operation. The modeled period must cover the entire history of the well field production to represent the transient groundwater flow paths resulting from groundwater pumping. The measured tracers then provide an objective for calibrating such numerical models at the time of tracer sampling.

[72] The groundwater age distributions of the Holten well field show that the shallow production wells are very vulnerable to surface contamination, having an age of less than 20 years for more than 75% of pumped groundwater. This short travel time will also cause these wells to respond quickly to reductions in surface loads from agriculture [*Broers et al*., 2004]. The decreasing nitrate concentrations found in these wells confirm this expected response [*Broers et al*., 2012]. The contaminant loads from agriculture and geochemical properties of the subsurface in the capture zone of the production well field can be characterized by the water quality data from the monitoring well field in combination with the ^{3}H/^{3}He ages at these screens [*Visser et al*., 2009a].

[73] A large proportion of the water pumped by the deep production wells is older than 60 years. The apparent ^{39}Ar age of this old fraction is at the centennial rather than millennial scale. As a result, sustained agricultural practices will likely impact the water quality in the deep aquifer and its contribution to the Holten well field. These aspects of the age distribution of a drinking water production well field are key to understanding observed trends in contaminants, to predict future trends to support well field management decisions (continue, deepen, abandon, or treat), and to guide capture zone protection measures.

5. Conclusions

[74] Deriving a groundwater age distribution requires multiple tracers, especially if the shape of the distribution cannot be assumed to follow a particular mathematical model. This is the case for wells in a drinking water production well field that influence each other by competing for capture area. A novel application of a discrete groundwater age distribution model appears to be capable of capturing the shape of the groundwater age distribution. ^{3}H/^{3}He ages from monitoring wells in the vicinity of the well field provide the age stratification of the aquifer surrounding the well field. The comparison of the age distribution of pumped groundwater and the age stratification in the aquifer shows that the well field as a whole preferentially captures groundwater from shallower formations with higher hydraulic conductivity.

[75] **Acknowledgments.** The authors are grateful for the permission, support, and funding (25%) from Vitens Water, owner and operator of the Holten well field. This study was cofunded by the Department of Economic Affairs of the Netherlands. We appreciate the support of "Bundesamt für Strahlenschutz (Germany)" that provided the measurements of the atmospheric ^{85}Kr input activities. We thank Kip Solomon and Alan Rigby for providing thoughtful discussion on the interpretation of the diffusion sampler data. Elaborate comments from W. Aeschbach-Hertig, two anonymous reviewers, and the Associate Editor enabled us to improve the quality of the manuscript. Part of this work was performed under the auspices of the U.S. Department of Energy by Lawrence Livermore National Laboratory under contract DE-AC52-07NA27344. LLNL-JRNL-635812.

References

Aeschbach-Hertig, W., F. Peeters, U. Beyerle, and R. Kipfer (1999), Interpretation of dissolved atmospheric noble gases in natural waters, *Water Resour. Res.*, *35*(9), 2779–2792.

Aeschbach-Hertig, W., F. Peeters, U. Beyerle and R. Kipfer (2000), Palaeotemperature reconstruction from noble gases in ground water taking into account equilibration with entrapped air, *Nature*, *405*(6790), 1040–1044.

Aeschbach-Hertig, W., H. El-Gamal, M. Wieser, and L. Palcsu (2008), Modeling excess air and degassing in groundwater by equilibrium partitioning with a gas phase, *Water Resour. Res.*, *44*, W08449, doi:10.1029/2007WR006454.

Ballentine, C. J., and C. M. Hall (1999), Determining paleotemperature and other variables by using an error-weighted, nonlinear inversion of noble gas concentrations in water, *Geochim. Cosmochim. Acta*, *63*(16), 2315–2336.

Batlle-Aguilar, J., et al. (2007), Identification of groundwater quality trends in a chalk aquifer threatened by intensive agriculture in Belgium, *Hydrogeol. J.*, *15*(8), 1615–1627.

Böhlke, J. K. (2002), Groundwater recharge and agricultural contamination, *Hydrogeol. J.*, *10*(1), 153–179.

Brennwald, M. S., R. Kipfer, and D. M. Imboden (2005), Release of gas bubbles from lake sediment traced by noble gas isotopes in the sediment pore water, *Earth Planet. Sci. Lett.*, *235*(1–2), 31–44.

Broers, H. P., and B. Van der Grift (2004), Regional monitoring of temporal changes in groundwater quality, *J. Hydrol.*, *296*(1–4), 192–220.

Broers, H. P., and F. C. Van Geer (2005), Monitoring strategies at phreatic wellfields: A 3D travel time approach, *Ground Water*, *43*(6), 850–862.

Broers, H. P., J. Rozemeijer, M. Van De Aa, B. Van Der Grift, and E. A. Buijs (2004), Groundwater quality trend detection at the regional scale: Effects of spatial and temporal variability, in *Proceeding of the 4th international Groundwater Quality Conference*, vol. *297*, p. 50–60, Int. Assoc. of Hydrol. Sci.-Assoc. Int. des Sci. Hydrol. Publ., Waterloo, Canada.

Broers, H. P., B. Van Der Grift, J. Griffioen, and R. Heerdink (2007), Modelling reactive transport of diffuse contaminants: Identifying the groundwater contribution to surface water quality, in *Groundwater Science and Policy*, edited by P. Quevauviller, pp. 630–644, R. Soc. of Chem., London, U. K.

Broers, H. P., R. Heerdink, A. Visser, and A. Marsman (2012), Aquatempo: Groundwater dating for public water supply wells, *TNO Rep. 2012-R10374* (in Dutch), 103 pp., TNO, Utrecht, Netherlands.

Busenberg, E., and L. N. Plummer (1992), Use of chlorofluorocarbons (CCl_3F and CCl_2F_2) as hydrologic tracers and age-dating tools: The alluvium and terrace system of central Oklahoma, *Water Resour. Res.*, *28*(9), 2257–2283.

Busenberg, E., and L. N. Plummer (2000), Dating young groundwater with sulfur hexafluoride: Natural and anthropogenic sources of sulfur hexafluoride, *Water Resour. Res.*, *36*(10), 3011–3030.

Byrd, R. H., P. Lu, J. Nocedal, and C. Zhu (1995), A limited memory algorithm for bound constrained optimization, *SIAM J. Sci. Comput.*, *16*(5), 1190–1208.

Cirpka, O. A., M. N. Fienen, M. Hofer, E. Hoehn, A. Tessarini, R. Kipfer, and P. K. Kitanidis (2007), Analyzing bank filtration by deconvoluting time series of electric conductivity, *Ground Water*, *45*(3), 318–328.

Cole, B. E., and S. E. Silliman (1997), Capture zones for passive wells in heterogeneous unconfined aquifers, *Ground Water*, *35*(1), 92–98.

Cole, B. E., and S. E. Silliman (2000), Utility of simple models for capture zone delineation in heterogeneous unconfined aquifers, *Ground Water*, *38*(5), 665–672.

Corcho Alvarado, J. A., R. Purtschert, F. Barbecot, C. Chabault, J. Rueedi, V. Schneider, W. Aeschbach-Hertig, R. Kipfer, and H. H. Loosli (2007), Constraining the age distribution of highly mixed groundwater using ^{39}Ar: A multiple environmental tracer ($^3H/^3He$, ^{85}Kr, ^{39}Ar, and ^{14}C) study in the semiconfined Fontainebleau Sands Aquifer (France), *Water Resour. Res.*, *43*, W03427, doi:10.1029/2006WR005096.

De Louw, P. G. B., Y. van der Velde, and S. E. A. T. M. van der Zee (2011), Quantifying water and salt fluxes in a lowland polder catchment dominated by boil seepage: A probabilistic end-member mixing approach, *Hydrol. Earth Syst. Sci.*, *15*(7), 2101–2117.

Duffy, C. J., and D.-H. Lee (1992), Base flow response from nonpoint source contamination: Simulated spatial variability in source, structure, and initial condition, *Water Resour. Res.*, *28*(3), 905–914.

Eberts, S. M., J. K. Böhlke, L. J. Kauffman, and B. C. Jurgens (2012), Comparison of particle-tracking and lumped-parameter age-distribution models for evaluating vulnerability of production wells to contamination, *Hydrogeol. J.*, *20*(2), 263–282.

Engesgaard, P., K. H. Jensen, J. Molson, E. O. Frind, and H. Olsen (1996), Large-scale dispersion in a sandy aquifer: Simulation of subsurface transport of environmental tritium, *Water Resour. Res.*, *32*(11), 3253–3266.

Etcheverry, D., and P. Perrochet (2000), Direct simulation of groundwater transit-time distributions using the reservoir theory, *Hydrogeol. J.*, *8*(2), 200–208.

EU (2006), Directive 2006/118/EC on the Protection of Groundwater against Pollution and Deterioration, European Union, Brussels, Belgium.

Fontes, J. C., and J. M. Garnier (1979), Determination of the initial ^{14}C activity of the total dissolved carbon: A review of the existing model and a new approach, *Water Resour. Res.*, *15*(2), 399–413.

Foster, S. S. D., A. C. Cripps, and A. Smith-Carington (1982), Nitrate leaching to groundwater, *Philos. Trans. R. Soc. London B*, *296*(1082), 477–489.

Frind, E. O., D. S. Muhammad, and J. W. Molson (2002), Delineation of three-dimensional well capture zones for complex multi-aquifer systems, *Ground Water*, *40*(6), 586–598.

Gardner, P., and D. K. Solomon (2009), An advanced passive diffusion sampler for the determination of dissolved gas concentrations, *Water Resour. Res.*, *45*, W06423, doi:10.1029/2008WR007399.

Gehrels, J. C., J. E. M. Peeters, J. J. De Vries, and M. Dekkers (1998), The mechanism of soil water movement as inferred from ^{18}O stable isotope studies, *Hydrol. Sci. J.*, *43*(4), 579–594.

Gelhar, L. W., C. Welty, and K. R. Rehfeldt (1992), A critical review of data on field-scale dispersion in aquifers, *Water Resour. Res.*, *28*(7), 1955–1974.

Green, C. T., J. K. Böhlke, B. A. Bekins, and S. P. Phillips (2010), Mixing effects on apparent reaction rates and isotope fractionation during denitrification in a heterogeneous aquifer, *Water Resour. Res.*, *46*, W08525, doi:10.1029/2009WR008903.

Griffioen, J., et al. (2002), *Spatial Developments and Groundwater Management. Groundwater Quality, Surface Load and Geochemical Processes (DR 3) (in Dutch)*, NITG-TNO & R. Haskoning, Utrecht, Netherlands.

Griffioen, J., et al. (2003), *Spatial Developments and Groundwater Management. Initial Situation of the Holten Public Drinking Water Supply Well Field (DR 5) (in Dutch)*, NITG-TNO & R. Haskoning, Utrecht, Netherlands.

Harrar, W. G., T. O. Sonnenborg, and H. J. Henriksen (2003), Capture zone, travel time, and solute-transport predictions using inverse modeling and different geological models, *Hydrogeol. J.*, *11*(5), 536–548.

Heaton, T. H. E., and J. C. Vogel (1981), ''Excess air'' in groundwater, *J. Hydrol.*, *50*, 201–216.

Hinsby, K., A. L. Højberg, P. Engesgaard, K. H. Jensen, F. Larsen, L. N. Plummer, and E. Busenberg (2007), Transport and degradation of chlorofluorocarbons (CFCs) in the pyritic Rabis Creek aquifer, Denmark, *Water Resour. Res.*, *43*, W10423, doi:10.1029/2006WR005854.

IAEA/WMO (2010), Global Network of Isotopes in Precipitation, The GNIP Database, http://isohis.iaea.org. Vienna, Austria.

Ivey, S. S., R. W. Gentry, D. Larsen, and J. Anderson (2008), Inverse application of age-distribution modeling using environmental tracers $^3H/^3He$, *J. Hydrol. Eng.*, *13*(11), 1002–1010.

Iwaco (1993), Study on the recharge areas of the drinking water abstractions in the province of Overijssel (in Dutch), Final Rep. 22.0641.0, Phase 2, 27 pp., Iwaco, Groningen, Netherlands.

Johnson, N. L., S. Kotz, and N. Balakrishnan (1995), *Continuous Univariate Distributions*, vol. *1*, chap. 18 and vol. 2, chap. 29, Wiley, New York.

Jurgens, B. C., J. K. Böhlke, and S. M. Eberts (2012), TracerLPM (Version 1): An Excel® workbook for interpreting groundwater age distributions from environmental tracer data, *U.S. Geol. Surv. Tech. and Methods Rep. 4-F3*, 60 pp., U.S. Geol. Surv., Reston, Va.

Kalin, R. M. (1999), Radiocarbon dating of groundwater systems, in *Environmental Tracers in Subsurface Hydrology*, edited by P. G. Cook and A. Herczeg, pp. 111–144, Springer, New York.

KNMI (2012), Climate Atlas Longterm Averages 1981–2010, KNMI, De Bilt, Netherlands. [Available at http://www.klimaatatlas.nl/.]

Laier, T. (2004), Nitrate monitoring and CFC-age dating of shallow groundwaters—An attempt to check the effect of restricted use of fertilizers, in *Nitrate in Groundwaters, IAH Selected Papers on Hydrogeology*, edited by L. Razowska-Jaworek and A. Sadurski, pp. 247–258, A. A. Balkema, Leiden, Netherlands.

Landon, M. K., C. T. Green, K. Belitz, M. J. Singleton, and B. K. Esser (2011), Relations of hydrogeologic factors, groundwater reduction-oxidation conditions, and temporal and spatial distributions of nitrate, Central-Eastside San Joaquin Valley, California, USA, *Hydrogeol. J.*, *19*(6), 1203–1224.

Larocque, M., P. G. Cook, K. Haaken, and C. T. Simmons (2009), Estimating flow using tracers and hydraulics in synthetic heterogeneous aquifers, *Ground Water*, *47*(6), 786–796.

Loosli, H. H. (1983), A dating method with ^{39}Ar, *Earth Planet. Sci. Lett.*, *63*(1), 51–62.

Loosli, H. H., B. E. Lehmann, and W. Balderer (1989), Argon-39, argon-37 and krypton-85 isotopes in Stripa groundwaters, *Geochim. Cosmochim. Acta*, *53*(8), 1825–1829.

Maloszewski, P., and A. Zuber (1982), Determining the turnover time of groundwater systems with the aid of environmental tracers. 1. Models and their applicability, *J. Hydrol.*, *57*(3–4), 207–231.

Maloszewski, P., and A. Zuber (1993), Principles and practice of calibration and validation of mathematical models for the interpretation of environmental tracer data in aquifers, *Adv. Water Resour.*, *16*(3), 173–190.

Maloszewski, P., and A. Zuber (1998), A general lumped parameter model for the interpretation of tracer data and transit time calculation in hydrologic systems—Comments, *J. Hydrol.*, *204*(1–4), 297–300.

Manning, A. H., D. K. Solomon, and A. L. Sheldon (2003), Applications of a total dissolved gas pressure probe in ground water studies, *Ground Water*, *41*(4), 440–448.

Manning, A. H., D. Kip Solomon, and S. A. Thiros (2005), H-3/He-3 age data in assessing the susceptibility of wells to contamination, *Ground Water*, *43*(3), 353–367.

Massoudieh, A., S. Sharifi, and D. K. Solomon (2012), Bayesian evaluation of groundwater age distribution using radioactive tracers and anthropogenic chemicals, *Water Resour. Res.*, *48*, W09529, doi:10.1029/2012WR011815.

Meinardi, C. R. (1994), Groundwater recharge and travel times in the sandy regions of the Netherlands, PhD thesis, 211 pp., VU Univ., Amsterdam.

Mendizabal, I., and P. J. Stuyfzand (2011), Quantifying the vulnerability of well fields towards anthropogenic pollution: The Netherlands as an example, *J. Hydrol.*, *398*(3–4), 260–276.

Molénat, J., and C. Gascuel-Odoux (2002), Modelling flow and nitrate transport in groundwater for the prediction of water travel times and of consequences of land use evolution on water quality, *Hydrol. Processes*, *16*(2), 479–492.

Mook, W. G. (1980), Carbon-14 in hydrogeological studies, in Handbook of Environmental Isotope Geochemistry, vol. *1*, edited by P. Fritz and J. C. Fontes, pp. 49–74, Elsevier, New York.

Neumann, R. B., E. M. LaBolle, and C. F. Harvey (2008), The effects of dual-domain mass transfer on the tritium/helium-3 dating method, *Environ. Sci. Technol.*, *42*(13), 4837–4843.

Nolan, B. T., B. C. Ruddy, K. J. Hitt, and D. R. Helsel (1997), Risk of nitrate in groundwaters of the United States—A national perspective, *Environ. Sci. Technol.*, *31*(8), 2229–2236.

Oeschger, H., A. Gugelman, H. Loosi, U. Schotterer, U. Siegenthaler, and W. Wiest (1974), 39Ar dating of groundwater, paper presented at IAEA Symposium on *Isotope Techniques in Groundwater Hydrology*, 11–15 March 1974, pp. 179–190, Int. At. Energy Agency, Vienna.

Osenbrück, K., S. Fiedler, K. Knöller, S. M. Weise, J. Sültenfuß, H. Oster, and G. Strauch (2006), Timescales and development of groundwater pollution by nitrate in drinking water wells of the Jahna-Aue, Saxonia, Germany, *Water Resour. Res.*, *42*, W12416, doi:10.1029/2006WR004977.

Plummer, L. N., E. Busenberg, J. K. Böhlke, D. L. Nelms, R. L. Michel, and P. Schlosser (2001), Groundwater residence times in Shenandoah National Park, Blue Ridge Mountains, Virginia, USA: A multi-tracer approach, *Chem. Geol.*, *179*(1–4), 93–111.

Poreda, R. J., T. E. Cerling, and D. K. Salomon (1988), Tritium and helium-isotopes as hydrologic tracers in a shallow unconfined aquifer, *J. Hydrol.*, *103*(1–2), 1–9.

Purtschert, R., H. H. Loosli, U. Beyerle, W. Aeschbach-Hertig, D. Imboden, R. Kipfer, and R. Wieler (1999), Dating of young water components by combined application of 3H/3He and 85Kr measurements, paper presented at IAEA Symposium on Isotope Techniques in Water Resources Development and Management, 10–14 May 1999, Int. At. Energy Agency, Vienna, Austria.

Rock, G., and H. Kupfersberger (2002), Numerical delineation of transient capture zones, *J. Hydrol.*, *269*(3–4), 134–149.

Roether, W. (1967), *Estimating the Tritium Input to Groundwater From Wine Samples: Groundwater and Direct Run-Off Contribution to Central European Surface Waters*, pp. 73–91, Int. At. Energy Agency, Vienna.

Ruijpers, L., B. van der Grift, B. van Breukelen, and J. Griffioen (2004), The evolution of groundwater quality around pumping-station Holten, the Netherlands, simulated by means of the multi-component geochemical transport model PHT3D, TNO Rep. NITG 04-265-A, TNO-NITG, Utrecht, Netherlands.

Sanford, W. (2011), Calibration of models using groundwater age, *Hydrogeol. J.*, *19*(1), 13–16.

Schlosser, P., M. Stute, H. Dörr, C. Sonntag, and K. O. Münnich (1988), Tritium/^{3}He dating of shallow groundwater, *Earth Planet. Sci. Lett.*, *89*(3–4), 353–362.

Sebol, L. A., W. D. Robertsona, E. Busenbergb, L. N. Plummerb, M. C. Ryanc, and S. L. Schiff (2007), Evidence of CFC degradation in groundwater under pyrite-oxidizing conditions, *J. Hydrol.*, *347*(1–2), 1–12.

Smethie, W. M., Jr., D. K. Solomon, S. L. Schiff, and G. G. Mathieu (1992), Tracing groundwater flow in the Borden aquifer using krypton-85, *J. Hydrol.*, *130*(1–4), 279–297.

Solomon, D. K., A. Hunt, and R. J. Poreda (1996), Source of radiogenic helium 4 in shallow aquifers: Implications for dating young groundwater, *Water Resour. Res.*, *32*(6), 1805–1813.

Spalding, R. F., and M. E. Exner (1993), Occurrence of nitrate in groundwater—A review, *J. Environ. Qual.*, *22*(3), 392–402.

Strebel, O., W. H. M. Duynisveld, and J. Böttcher (1989), Nitrate pollution of groundwater in western Europe, *Agric. Ecosyst. Environ.*, *26*(3–4), 189–214.

Stute, M., M. Forster, H. Frischkorn, A. Serejo, J. F. Clark, P. Schlosser, W. S. Broecker, and G. Bonani (1995), Cooling of tropical Brazil (5°C) during the last glacial maximum, *Science*, *269*(5222), 379–383.

Suckow, A. (2012), Lumped Parameter Modelling of Age Distributions Using Up to Two Parallel Black Boxes, Manual, Version 2.1. CSIRO Land and Water, Australia.

Sültenfuß, J., W. Roether, and M. Rhein (2004), The Bremen mass spectrometric facility for the measurement of helium isotopes, neon, and tritium in water, paper presented at IAEA International Symposium on Quality Assurance for Analytical Methods in Isotope Hydrology, Int. At. Energy Agency, Vienna.

Sültenfuß, J., R. Purtschert, and J. F. Führböter (2011), Age structure and recharge conditions of a coastal aquifer (northern Germany) investigated with ^{39}Ar, ^{14}C, ^{3}H, He isotopes and Ne, *Hydrogeol. J.*, *19*(1), 221–236.

Tesoriero, A. J., H. Liebscher, and S. E. Cox (2000), Mechanism and rate of denitrification in an agricultural watershed: Electron and mass balance along groundwater flow paths, *Water Resour. Res.*, *36*(6), 1545–1559.

Tikhonov, A. N., and V. A. Arsenin (1977), *Solutions of Ill-Posed Problems*, Winston & Sons, Washington.

Troldborg, L., K. H. Jensen, P. Engesgaard, J. C. Refsgaard, and K. Hinsby (2008), Using environmental tracers in modeling flow in a complex shallow aquifer system, *J. Hydrol. Eng.*, *13*(11), 1037–1048.

Van den Brink, C., W. J. Zaadnoordijk, B. van der Grift, P. C. de Ruiter, and J. Griffioen (2008), Using a groundwater quality negotiation support system to change land-use management near a drinking-water abstraction in the Netherlands, *J. Hydrol.*, *350*(3–4), 339–356.

Van der Velde, Y., P. J. J. F. Torfs, S. E. A. T. M. van der Zee, and R. Uijlenhoet (2012), Quantifying catchment-scale mixing and its effect on time-varying travel time distributions, *Water Resour. Res.*, *48*, W06536, doi:10.1029/2011WR011310.

Visser, A., et al. (2007), Dating degassed groundwater with ^{3}H/^{3}He, *Water Resour. Res.*, *43*, WR10434, doi:10.1029/2006WR005847.

Visser, A., et al. (2009a), Trends in pollutant concentrations in relation to time of recharge and reactive transport at the groundwater body scale, *J. Hydrol.*, (3–4), 427–439.

Visser, A., et al. (2009b), Comparison of methods for the detection and extrapolation of trends in groundwater quality, *J. Environ. Monit.*, *11*, 2030–2043.

Visser, A., et al. (2009c), Travel time distributions derived from particle tracking in models with weak sinks, *Ground Water*, *47*(2), 237–245.

Visser, A., et al. (2009d), Degassing of ^{3}H/^{3}He, CFCs and SF_6 by denitrification: Measurements and two-phase transport simulations, *J. Contam. Hydrol.*, *103*(3–4), 206–218.

Vogel, J. C. (1967), Investigation of groundwater flow with radiocarbon, paper presented at IAEA Symposium on Isotopes in Hydrology, 14–18 November 1966, Int. At. Energy Agency, Vienna, Austria.

WHO (2006), *Protecting Groundwater for Health*, IWA Publ., London.

Winger, K., J. Feichter, M. B. Kalinowski, H. Sartorius, and C. Schlosser (2005), A new compilation of the atmospheric ^{85}krypton inventories from 1945 to 2000 and its evaluation in a global transport model, *J. Environ. Radioactiv.*, *80*(2), 183–215.

Zhang, Y.-C., C. P. Slomp, H. P. Broers, H. F. Passier, and P. Van Cappellen (2009), Denitrification coupled to pyrite oxidation and changes in groundwater quality in a shallow sandy aquifer, *Geochim. Cosmochim. Acta*, *73*(22), 6716–6726.

Zuber, A., K. Różański, J. Kania, and R. Purtschert (2011), On some methodological problems in the use of environmental tracers to estimate hydrogeologic parameters and to calibrate flow and transport models, *Hydrogeol. J.*, *19*(1), 53–69.